

Deterministic quantum nonlinear optics with single atoms and virtual photons

Anton Frisk Kockum,^{1,*} Adam Miranowicz,^{1,2} Vincenzo Macrì,^{1,3} Salvatore Savasta,^{1,3} and Franco Nori^{1,4}

¹*Center for Emergent Matter Science, RIKEN, Saitama 351-0198, Japan*

²*Faculty of Physics, Adam Mickiewicz University, PL-61-614 Poznan, Poland*

³*Dipartimento di Scienze Matematiche e Informatiche, Scienze Fisiche e Scienze della Terra, Università di Messina, I-98166 Messina, Italy*

⁴*Physics Department, University of Michigan, Ann Arbor, Michigan 48109-1040, USA*

(Received 26 January 2017; published 29 June 2017)

We show how analogs of a large number of well-known nonlinear-optics phenomena can be realized with one or more two-level atoms coupled to one or more resonator modes. Through higher-order processes, where virtual photons are created and annihilated, an effective deterministic coupling between two states of such a system can be created. In this way, analogs of three-wave mixing, four-wave mixing, higher-harmonic and -subharmonic generation (i.e., up- and down-conversion), multiphoton absorption, parametric amplification, Raman and hyper-Raman scattering, the Kerr effect, and other nonlinear processes can be realized. In contrast to most conventional implementations of nonlinear optics, these analogs can reach unit efficiency, only use a minimal number of photons (they do not require any strong external drive), and do not require more than two atomic levels. The strength of the effective coupling in our proposed setups becomes weaker the more intermediate transition steps are needed. However, given the recent experimental progress in ultrastrong light-matter coupling and improvement of coherence times for engineered quantum systems, especially in the field of circuit quantum electrodynamics, we estimate that many of these nonlinear-optics analogs can be realized with currently available technology.

DOI: 10.1103/PhysRevA.95.063849

I. INTRODUCTION

In nonlinear optics, a medium responds nonlinearly to incoming light of high intensity. This nonlinear response can give rise to a host of effects, including frequency conversion and amplification, many of which have important technological applications [1–4]. After the high-intensity light of a laser made possible the first experimental demonstration of second-harmonic generation (frequency up-conversion) in 1961 [5], many more nonlinear-optics effects were demonstrated using a variety of nonlinear media. The many applications and the fundamental nature of nonlinear optics have also inspired investigations of analogous effects in other types of waves. Prominent examples include nonlinear acoustics [6,7], nonlinear spin waves [8], nonlinear atom optics [9,10], nonlinear Josephson plasma waves [11], and nonlinear plasmonics [12]. Analogies of this kind can sometimes enable simulations or demonstrations of phenomena that are hard to realize in other systems [13–15].

In this article, we will show that analogs of many nonlinear-optics effects can also be realized by coupling one or more resonator modes to one or more two-level atoms. This stands in contrast to many other nonlinear-optics realizations, which require three or more atomic levels [4,16]. The key to the analogs we propose lies in the full interaction between a two-level atom and an electromagnetic mode, which is given by the quantum Rabi Hamiltonian [17]. This Hamiltonian includes terms that can change the number of excitations in the system, enabling higher-order processes via virtual photons. These photons are created and annihilated in a way that generates a deterministic coupling between two system states that otherwise do not have a direct coupling. In this

way, we can realize analogs of various frequency-conversion processes, parametric amplification, Raman and hyper-Raman scattering, multiphoton absorption, the Kerr effect, and other nonlinear processes.

Just as nonlinear-optics effects usually require very high light intensity to manifest clearly, the higher-order processes we consider require a very strong light-matter coupling to become noticeable. Specifically, the light-matter coupling must be strong enough to ensure that the effective deterministic coupling between system states, induced by the higher-order processes, becomes larger than the relevant decoherence rates in the system. Ultrastrong coupling (USC, where the coupling strength starts to become comparable to the resonance frequencies of the bare system components) between light and matter has only recently been reached in some solid-state experiments [18–36]. Among these systems, circuit quantum electrodynamics (QED) [16,37–39] has provided some of the clearest examples [19,20,29–32,34–36], including the largest reported coupling strength [31] and the first quantum simulations of the USC regime [34,35].

The experimental progress in USC physics has motivated many theoretical studies of the interesting new effects that occur in this regime [40–51]. Some previous [52–54] and concurrent [55,56] works explore processes in the USC regime where the number of excitations is not conserved, such as multiphoton Rabi oscillations [53] and a single photon exciting multiple atoms [54]. Several of these processes can be interpreted as analogs of nonlinear-optics phenomena.

In this work, we present a unified picture of these types of processes and their relation to nonlinear optics. We also provide many more examples which together allow us to make complete tables with translations between three- and four-wave mixing in nonlinear optics and analogous processes in USC systems. It should be noted that these analogs, many of which can be realized in one universal setup, do not use

*anton.frisk.kockum@gmail.com

propagating waves, but instead mix excitations in resonators and atoms of different frequencies. We emphasize that, unlike many processes in conventional nonlinear optics, our setups do not require any external drives, but instead realize analogs of wave mixing with a minimal number of photons and unit efficiency.

Given the versatility and technological maturity of the circuit QED setups, we expect them to become the primary experimental platform for realizing these deterministic nonlinear-optics analogs with single atoms and virtual photons. We believe that these deterministic analogs can find many important applications, including frequency conversion and the creation of superposition states for use in quantum information technology. Circuit QED is already one of the most well-developed platforms for quantum information processing [57], so adding the full capabilities of nonlinear optics at the single-photon level to the toolbox of this field could result in many new exciting possibilities. Indeed, the development of nonlinear optics with single photons has been the subject of much theoretical and experimental work recently due to the wealth of potential applications [58]. We note here that although our proposal does not use propagating waves, circuit QED setups with stationary photons that mimic linear-optics experiments for itinerant photons have already been proposed [59]. Several of the nonlinear-optics analogs given in the present work could be incorporated into such an architecture.

This article is organized as follows. In Sec. II, we give a brief overview of how nonlinear processes in optics usually occur. We then describe how analogous deterministic processes become possible in the quantum Rabi model. In Secs. III and IV, we discuss three- and four-wave mixing, respectively, and give details of the analogous deterministic processes that can be realized with resonators ultrastrongly coupled to qubits. Other nonlinear processes, including higher-harmonic generation, parametric processes, and the Kerr effect, are discussed in Sec. V. In Sec. VI, we estimate achievable effective coupling strengths and decoherence rates, showing that our proposals can be realized with state-of-the-art technology in circuit QED. We conclude in Sec. VII. Some details are left for the appendices: Appendix A expands on the classical mechanisms for some nonlinear-optics phenomena, Appendix B gives a derivation of the perturbation-theory formula used to calculate the strength of the effective coupling between initial and final states in our three- and four-wave-mixing analogs, and Appendix C contains details about a few four-wave-mixing processes not treated in the main text.

II. MECHANISMS FOR NONLINEARITY

A. Nonlinear optics

In conventional classical electro-optical processes, the polarization \mathbf{P} of a given medium induced by the applied electric field \mathbf{E} is linearly proportional to its strength, i.e., $\mathbf{P} = \epsilon_0 \chi \mathbf{E}$, where ϵ_0 is the vacuum permittivity and $\chi \equiv \chi^{(1)}$ is the linear susceptibility of the medium, which can be considered a scalar for linear, homogeneous, and isotropic dielectric media. Usually, the real and imaginary parts of χ describe, respectively, the refraction and damping of a light beam going through such medium.

For a strong electric field \mathbf{E} and nonlinear media, the above linear relation for the induced polarization is generalized to

$$\mathbf{P} = \epsilon_0 (\chi^{(1)} \mathbf{E} + \chi^{(2)} \mathbf{E}^2 + \chi^{(3)} \mathbf{E}^3 + \dots), \quad (1)$$

which is considered a core principle of nonlinear optics [1–4]. In Eq. (1), $\chi^{(2)}$ and $\chi^{(3)}$ are the second- and third-order nonlinear susceptibilities, respectively. In general, these susceptibilities are tensors $\chi_{kl}^{(1)}$, $\chi_{klm}^{(2)}$, and $\chi_{klmn}^{(3)}$. However, for simplicity, we consider them as scalars, which is usually valid for isotropic dielectric media.

Various nonlinear optical phenomena (including wave mixing) can be explained classically by recalling the nonlinear dependence of the induced polarization and electric-field strength, as given by Eq. (1). Standard examples include Pockels and Kerr effects, which are, respectively, linear and quadratic electro-optical phenomena, in which the induced polarization (and, thus, also the refractive index) of a medium is proportional to the amplitude and its square of the applied constant electric field.

For example, second-harmonic generation in a medium described by the second-order susceptibility $\chi^{(2)}$ can be described classically as follows. Assuming that a monochromatic scalar electric field $E(t) = E_0 \cos(\omega t)$ is applied to the medium, the second-order induced polarization $P^{(2)}$ of the medium is given by

$$\begin{aligned} P^{(2)} &= \epsilon_0 \chi^{(2)} E^2 = \epsilon_0 \chi^{(2)} E_0^2 \cos^2(\omega t) \\ &= \epsilon_0 \chi^{(2)} E_0^2 \left(\frac{1 + \cos(2\omega t)}{2} \right) \\ &= \frac{1}{2} \epsilon_0 \chi^{(2)} E_0^2 + \frac{1}{2} \epsilon_0 \chi^{(2)} E_0^2 \cos(2\omega t), \end{aligned} \quad (2)$$

where the first term in the last line describes frequency-independent polarization, while the second term in the last line describes the polarization oscillating at twice the frequency of the input field. This doubling of the input frequency can be interpreted as second-harmonic generation.

In Appendix A, we present a few additional pedagogical classical explanations, based on Eq. (1), of phenomena arising due to the $\chi^{(2)}$ and $\chi^{(3)}$ nonlinearities. In the following sections, we write down interaction Hamiltonians describing many of these nonlinear-optics phenomena to better compare them with our proposed analogous processes. However, it should be kept in mind that these interaction Hamiltonians only describe the higher-order interaction mediated by the $\chi^{(2)}$ and $\chi^{(3)}$ nonlinearities. The lower-order interaction due to the $\chi^{(1)}$ term remains and limits the efficiency of the higher-order processes.

B. The quantum Rabi model

The Hamiltonian for a single two-level atom (a qubit) coupled to a single resonator mode can be written as ($\hbar = 1$ here and in the rest of the article)

$$\hat{H} = \omega_a \hat{a}^\dagger \hat{a} + \omega_q \frac{\hat{\sigma}_z}{2} + \hat{H}_{\text{int}}. \quad (3)$$

In the quantum Rabi model [17], the interaction is given by

$$\hat{H}_{\text{int}}^{\text{Rabi}} = g(\hat{a} + \hat{a}^\dagger)\hat{\sigma}_x = g(\hat{a} + \hat{a}^\dagger)(\hat{\sigma}_- + \hat{\sigma}_+), \quad (4)$$

where g is the coupling strength. Here, and in the following parts of the paper that discuss deterministic realizations of nonlinear optics, we use the notation that \hat{a} , \hat{b} , \hat{c} , and \hat{d} are the annihilation operators of resonator modes with frequencies ω_a , ω_b , ω_c , and ω_d , respectively. In setups with a single qubit, or with several identical qubits, the qubit transition frequency is denoted ω_q . In setups with qubits having different transition frequencies, the frequencies are denoted ω_{q1} , ω_{q2} , etc. The qubit operators $\hat{\sigma}_z$ and $\hat{\sigma}_x = \hat{\sigma}_- + \hat{\sigma}_+$ are Pauli matrices; $\hat{\sigma}_-$ and $\hat{\sigma}_+$ are the qubit lowering and raising operators, respectively.

In the limit $g \ll \omega_a, \omega_q$, the terms $\hat{a}^\dagger \hat{\sigma}_+$ and $\hat{a} \hat{\sigma}_-$ in $H_{\text{int}}^{\text{Rabi}}$ can be neglected in the rotating-wave approximation (RWA), leading to the Jaynes-Cummings (JC) model [60]

$$\hat{H}_{\text{int}}^{\text{JC}} = g(\hat{a}\hat{\sigma}_+ + \hat{a}^\dagger\hat{\sigma}_-). \quad (5)$$

Note that in the JC model, the number of excitations is conserved. In the quantum Rabi model, the number of excitations can change, but their parity is conserved. However, the quantum Rabi model can be generalized to

$$\hat{H}_{\text{int}}^{\text{gen}} = g(\hat{a} + \hat{a}^\dagger)(\hat{\sigma}_x \cos \theta + \hat{\sigma}_z \sin \theta), \quad (6)$$

where θ parametrizes the amount of longitudinal and transversal couplings. This generalized quantum Rabi model does not impose any restrictions on the number of excitations. The Hamiltonian in Eq. (6) has been realized in experiments with USC of flux qubits to resonators [19,20,29,31]. In such setups with flux qubits, the flux-qubit Hamiltonian can be written as

$$H_{\text{q}} = \frac{\epsilon \hat{\sigma}_z + \Delta \hat{\sigma}_x}{2}, \quad (7)$$

where $\hat{\sigma}_{z,x}$ are Pauli matrices in the qubit basis given by clockwise- and anticlockwise-circulating persistent currents $\pm I_p$ in the qubit loop, ϵ is an energy scale set by I_p and an external magnetic flux, and Δ is the tunneling energy between the two current states [61]. In this basis, the inductive coupling to the resonator is given by

$$H_{\text{int}} = g_{\text{ind}}(\hat{a} + \hat{a}^\dagger)\hat{\sigma}_z, \quad (8)$$

where the coupling strength g_{ind} is set by I_p , the zero-point current fluctuations in the resonator, and the mutual inductance in the circuit. By rotating to the energy eigenbasis of the qubit, one arrives at the interaction in Eq. (6) [19,20,29,31,62–64]. The parameter θ can be tuned by changing ϵ or Δ .

All these models can be straightforwardly extended to include additional resonators and qubits. The presence of one or more qubits provides the necessary nonlinearity to realize various deterministic analogs of nonlinear-optics processes that we will discuss in this article. For some of these processes, such as three-wave mixing (see Sec. III), the number of excitations changes by one; this requires setups with the generalized quantum Rabi model and its extensions. For other processes, e.g., four-wave mixing (see Sec. IV), the number of excitations changes by an even number or not at all; these processes can be realized with extensions of the standard quantum Rabi model or of the JC model, respectively. The fact that we need to break the parity symmetry of the standard quantum Rabi model for the three-wave-mixing analogs, but not for the four-wave-mixing case, is reminiscent of how, in

conventional nonlinear optics, inversion symmetry must be broken to realize $\chi^{(2)}$ processes, but $\chi^{(3)}$ processes can occur without breaking that symmetry [4].

In a majority of the nonlinear-optics analogs considered in this article, higher-order processes, mediated by the interaction Hamiltonians in Eqs. (4)–(6) (and their extensions to additional resonators and qubits), connect an initial state $|i\rangle$ with a final state $|f\rangle$ of the same energy through an effective interaction Hamiltonian

$$\hat{H}_{\text{int}}^{\text{eff}} = g_{\text{eff}}|f\rangle\langle i| + \text{H.c.}, \quad (9)$$

where g_{eff} is the strength of the effective coupling and H.c. denotes the Hermitian conjugate of the preceding terms. In many of the intermediate transitions that contribute to this effective coupling, virtual photons are created and destroyed. We provide a multitude of examples of this in the following sections. It is important to note here that the resonance between $|i\rangle$ and $|f\rangle$ can be set up such that all other states $|j\rangle$ which potentially could be reached through lower-order processes are far off resonance. In this way, the influence of lower-order processes can be made negligible, resulting in the higher-order process given by Eq. (9) reaching unit efficiency.

To calculate the effective coupling strength g_{eff} analytically, three different techniques have been employed in previous works. In Ref. [65], an effective Hamiltonian with explicit up- and down-conversion terms was derived through a series of unitary transformations combined with approximations that only retained terms of lowest order in $g_j/|\omega_n - \omega_m|$, where g_j are the relevant coupling strengths in the setup and $|\omega_n - \omega_m|$ are the energy differences of the relevant intermediate transitions. In Refs. [52,53,55], the intermediate virtual transitions were adiabatically eliminated, relying on the approximation that the population of the intermediate levels will not change significantly if $g_j \ll |\omega_n - \omega_m|$. In this article, we follow the approach of Ref. [54], which calculated g_{eff} using standard perturbation theory. Specifically, if the shortest path between $|i\rangle$ and $|f\rangle$ is an n th-order process, the effective coupling is given to lowest order by

$$g_{\text{eff}} = \sum_{j_1, j_2, \dots, j_{n-1}} \frac{V_{fj_{n-1}} \dots V_{j_2j_1} V_{j_1i}}{(E_i - E_{j_1})(E_i - E_{j_2}) \dots (E_i - E_{j_{n-1}})}, \quad (10)$$

where the sum goes over all virtual transitions forming n -step paths between $|i\rangle$ and $|f\rangle$, E_k denotes the energy of state $|k\rangle$, and $V_{km} = \langle k|\hat{H}_{\text{int}}|m\rangle$. A derivation of this formula is given in Appendix B.

In general, the perturbation-theory method of Eq. (10) appears to be the simplest way to calculate g_{eff} , especially for higher-order processes involving many virtual transitions. The other methods mentioned above can be more cumbersome, but provide more information such as energy-level shifts and higher-order corrections to the effective coupling.

III. THREE-WAVE MIXING

In this section, we look at three-wave mixing, starting with a general description of sum- and difference-frequency generation and then treating special cases such as up-conversion, down-conversion, and Raman scattering; see Fig. 1 for an

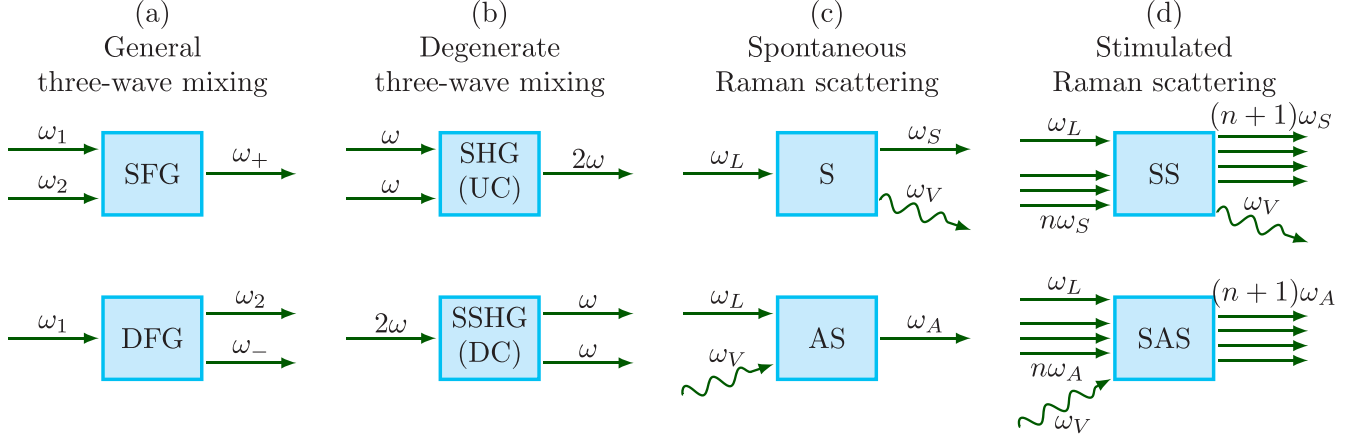


FIG. 1. Schematic representations (Feynman-like diagrams) of three-wave-mixing processes. (a) The two general types of three-wave mixing are sum-frequency generation (SFG, above) and difference-frequency generation (DFG, below). (b) When two of the involved frequencies are degenerate, we have either second-harmonic generation [SHG, or up-conversion (UC), above] or second-subharmonic generation [SSHG, or down-conversion (DC), below]. (c) Another special case is spontaneous Raman scattering, where a small part of the total energy is carried by a phonon (pictured as a wavy arrow), which is either outgoing [Stokes Raman scattering (S), above] or incoming [anti-Stokes Raman scattering (AS), also known as sideband cooling, below]. (d) In stimulated Raman scattering, the rate is increased due to the presence of n additional photons of the same frequency as the outgoing one. Stimulated Stokes Raman scattering (SS) is shown above and stimulated anti-Stokes Raman scattering (SAS) is shown below.

overview. We provide deterministic analogs based on the generalized quantum Rabi model for each case.

A. General description: Generation of sum- and difference-frequency fields

1. Nonlinear optics

The creation and annihilation of a photon with sum frequency ω_+ can be described in the Fock representation as $|n_1, n_2, n_+\rangle \rightarrow |n_1 - 1, n_2 - 1, n_+ + 1\rangle$ and $|n_1, n_2, n_+\rangle \rightarrow |n_1 + 1, n_2 + 1, n_+ - 1\rangle$, respectively; see also Fig. 1(a). The interaction Hamiltonian $\hat{H}_{\text{int}}^{(+)}$ for this sum-frequency generation can be given by

$$\hat{H}_{\text{int}}^{(+)} = g\hat{a}_1\hat{a}_2\hat{a}_+^\dagger + g^*\hat{a}_1^\dagger\hat{a}_2^\dagger\hat{a}_+, \quad (11)$$

in terms of the annihilation (\hat{a}_j) and creation (\hat{a}_j^\dagger) operators for the input modes (for $j = 1, 2$) and the output sum-frequency mode (for $j = +$), and the three-mode complex coupling constant g .

Analogously, the creation and annihilation of a photon with difference frequency ω_- can be described in the Fock representation as $|n_1, n_2, n_-\rangle \rightarrow |n_1 - 1, n_2 + 1, n_- + 1\rangle$ and $|n_1, n_2, n_-\rangle \rightarrow |n_1 + 1, n_2 - 1, n_- - 1\rangle$; see also Fig. 1(a). The interaction Hamiltonian $\hat{H}_{\text{int}}^{(-)}$ describing this process can be given by

$$\hat{H}_{\text{int}}^{(-)} = g\hat{a}_1\hat{a}_2^\dagger\hat{a}_-^\dagger + g^*\hat{a}_1^\dagger\hat{a}_2\hat{a}_-, \quad (12)$$

using the same notation as in Eq. (11) except that the subscript “+”, corresponding to the sum-frequency mode, is replaced by “-” for the difference-frequency mode.

The energy conservation principle implies that $\omega_+ = \omega_1 + \omega_2$ and $\omega_- = \omega_1 - \omega_2$, and the momentum conservation principle implies that $\mathbf{k}_+ = \mathbf{k}_1 + \mathbf{k}_2$ and $\mathbf{k}_- = \mathbf{k}_1 - \mathbf{k}_2$ for the wave vectors \mathbf{k}_j .

Note that in conventional nonlinear optics, the interaction Hamiltonians given here only describe the interaction that results from the higher-order $\chi^{(2)}$ nonlinearity. The full interaction Hamiltonian for the system will also contain lower-order terms, which limit the efficiency of the sum- and difference-frequency generation described by Eqs. (11) and (12).

2. Analogous processes

There are several possible setups that can realize analogs of sum- and difference-frequency generation deterministically. One such setup would be three resonators coupled to a single qubit using the generalized Rabi interaction in Eq. (6). If the resonator frequencies satisfy $\omega_a + \omega_b \approx \omega_c$, the two states $|1, 1, 0, g\rangle$ and $|0, 0, 1, g\rangle$ become resonant. Here, and in all the following discussions of deterministic processes, kets list photon excitation numbers, starting from the resonator with frequency ω_a , followed by qubit state(s) (g for ground state, e for excited state). The transition $|1, 1, 0, g\rangle \rightarrow |0, 0, 1, g\rangle$ then corresponds to sum-frequency generation [$a = 1, b = 2, c = +$ makes the connection explicit with Sec. III A 1 and Fig. 1(a)] and the transition $|0, 0, 1, g\rangle \rightarrow |1, 1, 0, g\rangle$ corresponds to difference-frequency generation [$a = 2, b = -, c = 1$].

The transition $|1, 1, 0, g\rangle \rightarrow |0, 0, 1, g\rangle$ is enabled by paths with several intermediate virtual transitions. One example of such a path is

$$|1, 1, 0, g\rangle \xrightarrow{\hat{b}\hat{\sigma}_+} |1, 0, 0, e\rangle \xrightarrow{\hat{c}^\dagger\hat{\sigma}_-} |1, 0, 1, g\rangle \xrightarrow{\hat{a}\hat{\sigma}_z} |0, 0, 1, g\rangle,$$

where the terms from Eq. (6) that generate the transitions are shown above the arrows. Note that the last transition changes the number of excitations in the system by one, which is only possible when the interaction is given by the generalized quantum Rabi Hamiltonian of Eq. (6). The last transition is also an example of how a virtual photon is annihilated

in the process. For the transition in the opposite direction (difference-frequency generation), a virtual photon is created instead.

By adiabatic elimination, or suitable unitary transformations combined with perturbation expansion in g over some frequency, it can be shown that these virtual transitions combine to give an effective interaction Hamiltonian

$$\hat{H}_{\text{int}}^{\text{eff}} = g_{\text{eff}} |0,0,1,g\rangle \langle 1,1,0,g| + \text{H.c.}, \quad (13)$$

where the effective coupling g_{eff} , in general, becomes weaker the more intermediate steps are needed. Later in this section, we will provide examples with detailed diagrams of the virtual transitions and calculations of the effective coupling.

In contrast to the interaction Hamiltonians for conventional nonlinear optics given in Sec. III A 1, the effective interaction given in Eq. (13) does not need to compete with lower-order processes if the transition energies in the system are chosen appropriately. For example, given the resonance condition $\omega_a + \omega_b \approx \omega_c$, the intermediate states $|1,0,0,e\rangle$ and $|1,0,1,g\rangle$, with energies $\omega_a + \omega_q$ and $\omega_a + \omega_c$, respectively, will be far off resonance as long as ω_q is chosen sufficiently far from ω_b . Thus, even though these intermediate states can be reached via lower-order processes, they will not become populated and will not limit the efficiency of the analog of three-wave mixing.

We note that, if at least one of the excitations in the three-wave mixing can be hosted in a qubit, other setups become possible. Both a single resonator coupled to two qubits and two resonators coupled to a single qubit could be used to implement the processes in Fig. 1(a). In particular, Ref. [54] analyzed the former case with $\omega_a \approx \omega_{q1} + \omega_{q2}$, showing an effective coupling between $|1,g,g\rangle$ and $|0,e,e\rangle$. In the latter case, the effective coupling of interest would be that between the states $|1,1,g\rangle$ and $|0,0,e\rangle$ when $\omega_a + \omega_b \approx \omega_q$.

B. Degenerate three-wave mixing: Second-harmonic and second-subharmonic generation

1. Nonlinear optics

Let us assume the degenerate process of three-wave mixing for which $\hat{a}_1 = \hat{a}_2 \equiv \hat{a}$ and $\omega_1 = \omega_2 \equiv \omega$. The energy conservation principle implies $\omega_+ = 2\omega$. The processes of the creation and annihilation of photons can be written as $|n,n_+\rangle \rightarrow |n-2,n_++1\rangle$ and $|n,n_+\rangle \rightarrow |n+2,n_+-1\rangle$; see also Fig. 1(b). The interaction Hamiltonian reads as

$$\hat{H}_{\text{int}} = g\hat{a}^2\hat{a}_+^\dagger + g^*\hat{a}^{\dagger 2}\hat{a}_+. \quad (14)$$

For second-harmonic generation (also referred to as up-conversion), one can assume that the initial pure state is $|\psi(t_0)\rangle = \sum_{n=0}^{\infty} c_n |n,0\rangle$. For second-subharmonic generation (also called down-conversion), one can assume that the initial pure state is $|\psi(t_0)\rangle = \sum_{n_+=0}^{\infty} c_{n_+} |0,n_+\rangle$. Here, c_n and c_{n_+} denote arbitrary complex superposition amplitudes satisfying the normalization conditions. It is seen that our description of second-subharmonic generation can be the same as that for second-harmonic generation except with a different initial state.

2. Analogous processes

(a) *Two resonators.* There are, again, several possible setups to realize analogs of up- and down-conversion deterministically. In Ref. [65], it was shown that an effective Hamiltonian like that of Eq. (14) can be achieved with two resonator modes coupled to a qubit with the interaction given by Eq. (6). However, in that work some additional assumptions were made, since ultrastrong coupling had not yet been experimentally demonstrated at the time. With strong enough coupling, the virtual transitions shown in the upper left panel of Fig. 2 combine to achieve a robust effective coupling between the states $|1,0,g\rangle$ and $|0,2,g\rangle$, which results in both up- and down-conversion. Note how virtual photons and qubit excitations are created or annihilated in all transitions marked with dashed arrows.

To be precise, the full Hamiltonian of the system is here given by

$$\hat{H} = \omega_a \hat{a}^\dagger \hat{a} + \omega_b \hat{b}^\dagger \hat{b} + \omega_q \frac{\hat{\sigma}_z}{2} + \hat{H}_{\text{int}}, \quad (15)$$

$$\begin{aligned} \hat{H}_{\text{int}} = & [g_a(\hat{a} + \hat{a}^\dagger) + g_b(\hat{b} + \hat{b}^\dagger)] \\ & \times (\hat{\sigma}_x \cos \theta + \hat{\sigma}_z \sin \theta), \end{aligned} \quad (16)$$

and the effective interaction due to the virtual transitions shown in Fig. 2 becomes

$$\hat{H}_{\text{int}}^{\text{eff}} = g_{\text{eff}} |1,0,g\rangle \langle 0,2,g| + \text{H.c.} \quad (17)$$

The effective coupling g_{eff} can be calculated with third-order perturbation theory. From Eq. (10), we have

$$g_{\text{eff}} = \sum_{n,m} \frac{\langle f | \hat{H}_{\text{int}} | n \rangle \langle n | \hat{H}_{\text{int}} | m \rangle \langle m | \hat{H}_{\text{int}} | i \rangle}{(E_i - E_n)(E_i - E_m)}. \quad (18)$$

Looking at the upper left panel of Fig. 2, we see that there are 12 paths contributing to the effective coupling between $|i\rangle = |0,2,g\rangle$ and $|f\rangle = |1,0,g\rangle$. Three of these paths consist solely of $\hat{\sigma}_z$ -mediated transitions (dashed red arrows in the figure). Their contribution is

$$\sqrt{2}g_a g_b \sin^3 \theta \left(\frac{1}{\omega_a \Delta_{ba}} - \frac{1}{\omega_b \Delta_{ba}} - \frac{1}{2\omega_b^2} \right), \quad (19)$$

where we introduced the notation $\Delta_{nm} = \omega_n - \omega_m$. This contribution sums to zero on resonance ($\omega_a = 2\omega_b$). The contribution from the remaining 9 paths is (introducing the notation $\Omega_{nm} = \omega_n + \omega_m$)

$$\begin{aligned} & \sqrt{2}g_a g_b \sin \theta \cos^2 \theta \left[\frac{1}{(\Delta_{ab} + \omega_q)\Omega_{aq}} - \frac{1}{\omega_a(\Delta_{ab} + \omega_q)} \right. \\ & - \frac{1}{(\Delta_{ab} + \omega_q)\Delta_{bq}} + \frac{1}{\omega_b(\Delta_{ab} + \omega_q)} - \frac{1}{\Delta_{ab}\Omega_{aq}} + \frac{1}{\Delta_{ab}\Delta_{bq}} \\ & \left. + \frac{1}{(2\omega_b - \omega_q)\Omega_{aq}} - \frac{1}{\omega_b(2\omega_b - \omega_q)} - \frac{1}{2\omega_b\Delta_{bq}} \right], \end{aligned} \quad (20)$$

which on resonance reduces to

$$g_{\text{eff}} = \frac{3\sqrt{2}g_a g_b \omega_q^2 \sin(2\theta) \cos \theta}{4\omega_b^4 - 5\omega_b^2 \omega_q^2 + \omega_q^4}. \quad (21)$$

Since the transition paths in the upper left panel of Fig. 2 go via two intermediate levels, g_{eff} becomes on the order

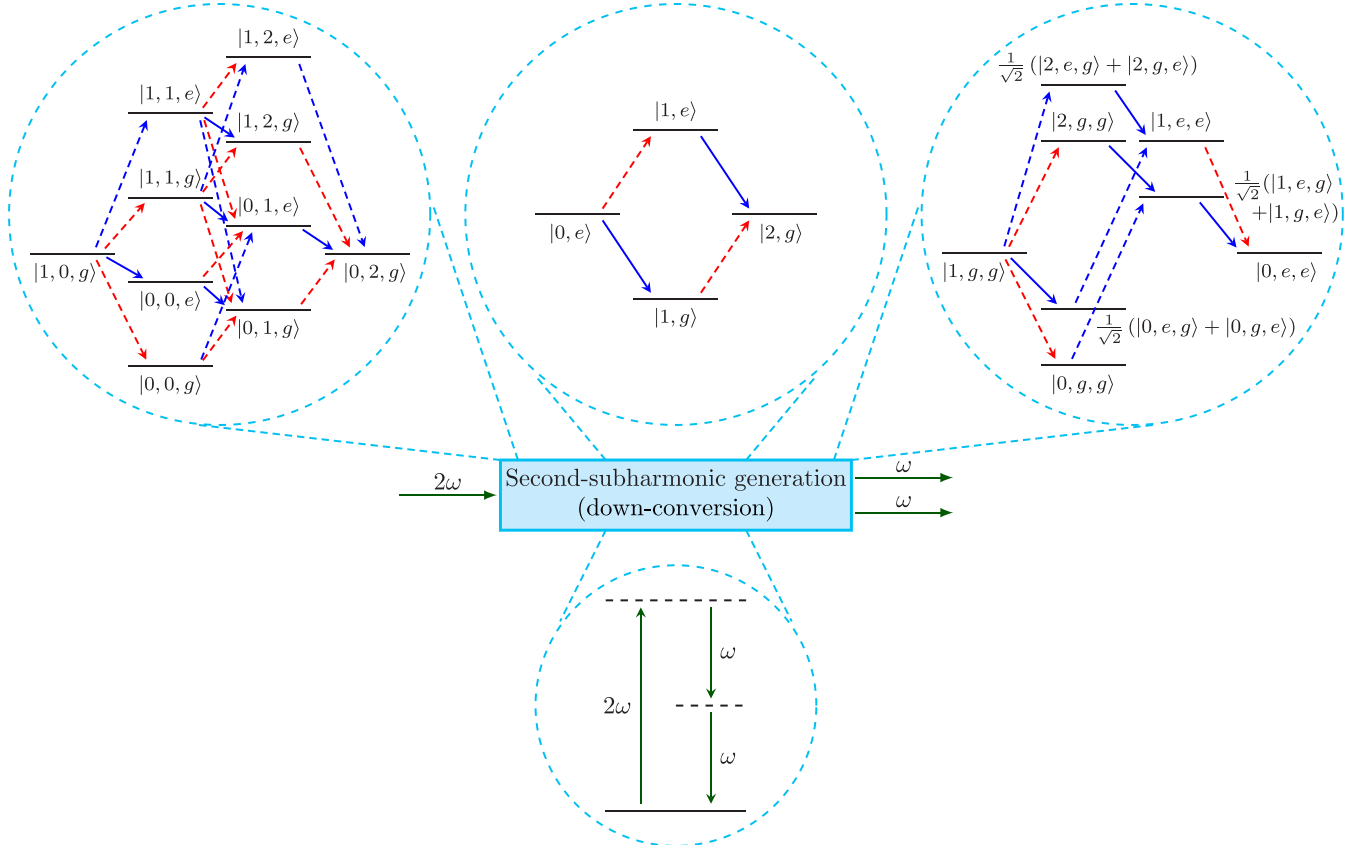


FIG. 2. Realizations of down- and up-conversion. The upper left panel shows all virtual transitions that contribute to the down-conversion process (second-subharmonic generation) $|1,0,g\rangle \rightarrow |0,2,g\rangle$ to lowest order. Blue solid arrows mark transitions that do *not* change the number of excitations [these transitions are mediated by the terms in the JC model, Eq. (5)], blue dashed arrows correspond to transitions that change the number of excitations by *two* [these transitions are mediated by the non-JC terms in the quantum Rabi model, Eq. (4)], and red dashed arrows show transitions that change the number of excitations by *one* [these transitions are mediated by the additional terms in the generalized Rabi model, Eq. (6)]. We have set $\omega_a = 2\omega_b$ and $\omega_q = 1.5\omega_b$. Similarly, the upper middle panel shows all virtual transitions that contribute to the down-conversion process $|0,e\rangle \rightarrow |2,g\rangle$ to lowest order. Here, we have set $\omega_q = 2\omega_a$. The upper right panel shows all virtual transitions that contribute to the down-conversion process $|1,g,g\rangle \rightarrow |0,e,e\rangle$ to lowest order. In this case, we have set $\omega_a = 2\omega_q$. Note that all intermediate energy levels in the upper panels are detuned far off resonance from the initial and final states, which means that lower-order processes will not be part of the effective interaction Hamiltonians given in the text of Sec. III B 2. The lower panel shows the generic level diagram for the process in nonlinear optics. Dashed horizontal lines denote virtual levels. If the directions of all arrows in the entire figure are reversed, up-conversion (second-harmonic generation) is shown instead.

of $(g_j/\omega)^2$ weaker than g_j ($j = a, b$). This expression is slightly more complicated than that derived in Ref. [65], where unitary transformations were combined with perturbation expansions using the additional simplifying assumptions that $g_b \ll |\omega_q - \omega_b| \ll \omega_a$.

A further demonstration of the effective coupling in Eq. (17) is given in Fig. 3, where we plot some of the energy levels in the system as a function of ω_a for the JC (dashed-dotted lines), Rabi (dashed lines), and generalized Rabi (solid lines) interactions. The inset shows a clear avoided crossing between $|1,0,g\rangle$ and $|0,2,g\rangle$; the splitting is set by g_{eff} . The JC and Rabi interactions do not give rise to such an avoided crossing since they cannot change the excitation number by one. However, all three interactions give rise to an avoided crossing between $|1,0,g\rangle$ and $|0,0,e\rangle$ to the left in the figure, since those two states have the same number of excitations.

(b) *Multiphoton Rabi oscillations.* An alternative implementation of up- and down-conversion is multiphoton Rabi

oscillations, illustrated in the upper middle panel of Fig. 2 and discussed in Ref. [53]. In this case, virtual transitions induce an effective coupling (and, thus, Rabi oscillations) between the states $|0,e\rangle$ and $|2,g\rangle$ for a single resonator coupled to a single qubit with $\omega_q \approx 2\omega_a$. The transitions are mediated by the generalized Rabi Hamiltonian Eq. (6) and give rise to an effective interaction

$$\hat{H}_{\text{int}}^{\text{eff}} = g_{\text{eff}}|0,e\rangle\langle 2,g| + \text{H.c.} \quad (22)$$

The effective coupling is easily calculated with second-order perturbation theory. With $|i\rangle = |2,g\rangle$ and $|f\rangle = |0,e\rangle$, Eq. (10) gives

$$g_{\text{eff}} = \sqrt{2}g^2 \sin \theta \cos \theta \left(\frac{1}{\Delta_{aq}} - \frac{1}{\omega_a} \right). \quad (23)$$

Using that on resonance $\omega_a = \omega_q/2$, this reduces to

$$g_{\text{eff}} = -2\sqrt{2} \sin(2\theta) \frac{g^2}{\omega_q}, \quad (24)$$

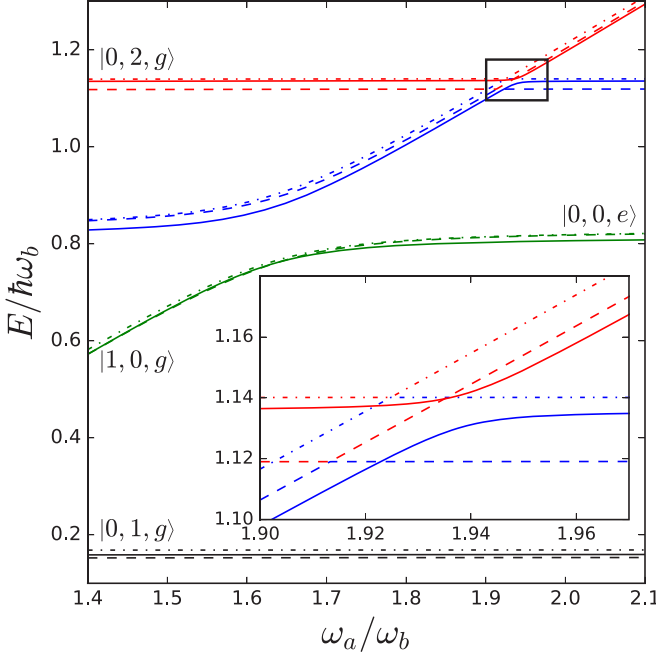


FIG. 3. Energy levels for two resonator modes coupled to a qubit via the JC [Eq. (5), dashed-dotted lines], quantum Rabi [Eq. (4), dashed lines], and generalized quantum Rabi [Eq. (6), solid lines] interactions, as a function of the resonance frequency ω_a of the first resonator mode. The inset shows a zoom-in of the area marked by the black rectangle in the upper right corner. Parameters: $\omega_q = 1.6\omega_b$, $g_a = 0.07\omega_b$, $g_b = 2g_a$, and $\theta = \pi/6$. The numerical simulations were performed in QuTiP [66,67].

which was also derived in Ref. [53] using adiabatic elimination. We note that the effective coupling acquires a factor g/ω_q due to the fact that each path between $|i\rangle$ and $|f\rangle$ contains one intermediate level.

(c) *Two identical qubits.* Yet another option, illustrated in the upper right panel of Fig. 2 and discussed in Ref. [54], is to couple a single resonator to two identical qubits such that the process $|1,g,g\rangle \leftrightarrow |0,e,e\rangle$ is realized. The Hamiltonian for this setup is

$$\hat{H} = \omega_a \hat{a}^\dagger \hat{a} + \sum_{j=1}^2 \omega_q \frac{\hat{\sigma}_z^{(j)}}{2} + \hat{H}_{\text{int}}, \quad (25)$$

$$\hat{H}_{\text{int}} = g(\hat{a} + \hat{a}^\dagger) \sum_{j=1}^2 (\hat{\sigma}_x^{(j)} \cos \theta + \hat{\sigma}_z^{(j)} \sin \theta), \quad (26)$$

and the effective interaction becomes

$$\hat{H}_{\text{int}}^{\text{eff}} = g_{\text{eff}} |1,g,g\rangle \langle 0,e,e| + \text{H.c.} \quad (27)$$

The third-order-perturbation-theory calculations for this process following Eq. (10) were already performed in the appendix of Ref. [54]. Here, we merely restate their result

$$g_{\text{eff}} = -\frac{8}{3} \frac{g^3}{\omega_q^2} \sin \theta \cos^2 \theta, \quad (28)$$

which is valid on resonance, when $\omega_a = 2\omega_q$. Again, we see that the effective coupling has a factor $(g/\omega)^2$, since each path contributing to the coupling contains two intermediate states.

In conclusion, we note that the multiphoton Rabi oscillation only requires two intermediate transitions, while the other two proposals require three. This means that the multiphoton Rabi oscillation has a larger effective coupling than the other two setups and is easier to implement.

C. Raman scattering

1. Nonlinear optics

In nonlinear optics, Raman scattering is a special case of nondegenerate three-wave mixing, mixing photons and optical phonons of the scattering nonlinear medium. Usually Raman scattering refers to the scattering of a light beam on optical phonons, which results in changing the frequency of the light beam [68]. We note that analogous scattering of photons on acoustic phonons is referred to as Brillouin scattering.

We consider the following fields: a driving laser (L) mode of frequency ω_L , a Stokes (S) mode of frequency ω_S , an anti-Stokes (A) mode of frequency ω_A , and optical vibrational phonon (V) modes of frequencies ω_{Vj} ($j = 1, 2, \dots$) as described by the corresponding creation (\hat{a}_k^\dagger) and annihilation (\hat{a}_k) operators for $k = L, A, S, Vj$.

(a) *Stokes Raman scattering.* Raman scattering with Stokes frequency $\omega_S < \omega_L$ is shortly referred to as Stokes (Raman) scattering. The process is illustrated in Fig. 1(c) and the interaction Hamiltonian can be written as

$$\hat{H}_{\text{int}}^{(S)} = \sum_j g_{Sj} \hat{a}_L \hat{a}_S^\dagger \hat{a}_{Vj}^\dagger + \text{H.c.}, \quad (29)$$

or its simpler single-phonon version

$$\hat{H}_{\text{int}}^{(S)} = g_S \hat{a}_L \hat{a}_S^\dagger \hat{a}_V^\dagger + \text{H.c.} \quad (30)$$

(b) *Anti-Stokes Raman scattering (sideband cooling).* One can also analyze the Raman scattering with anti-Stokes frequency $\omega_A > \omega_L$, referred to as anti-Stokes (Raman) scattering and illustrated in Fig. 1(c). The interaction Hamiltonian for the anti-Stokes Raman scattering can be written as

$$\hat{H}_{\text{int}}^{(A)} = \sum_j g_{Aj}^* \hat{a}_L \hat{a}_A^\dagger \hat{a}_{Vj} + \text{H.c.}, \quad (31)$$

or its simpler single-phonon version

$$\hat{H}_{\text{int}}^{(A)} = g_A^* \hat{a}_L \hat{a}_A^\dagger \hat{a}_V + \text{H.c.} \quad (32)$$

Since a phonon is absorbed in this process, it can also be referred to as sideband cooling of the phononic mode.

(c) *Stimulated Raman scattering.* The presence of additional photons in the S or A modes, as shown in Fig. 1(d), can increase the rate of Raman scattering. This is called stimulated Raman scattering. To further distinguish the processes in Fig. 1(c) from those in Fig. 1(d), the former can be referred to as spontaneous Raman scattering.

2. Analogous processes

We can achieve close analogs of Raman scattering in our deterministic setups by letting a qubit play the role of a phonon. The qubit is coupled to two resonators, one representing the

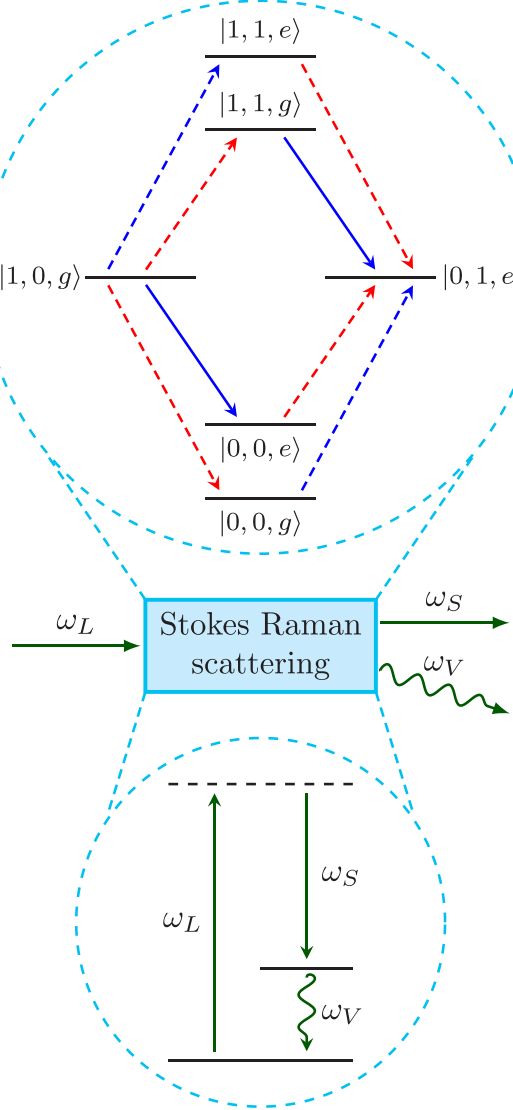


FIG. 4. Raman scattering and its deterministic analog. The upper panel shows all virtual transitions that contribute, to lowest order, to the process $|1,0,g\rangle \rightarrow |0,1,e\rangle$, which corresponds to Stokes Raman scattering. The lower panel shows the generic level diagram for the process in nonlinear optics. The same arrow and level styles as in Fig. 2 are used; we have set $\omega_a = 3\omega_q$ and $\omega_b = 2\omega_q$. If the directions of all arrows in the entire figure are reversed, and the labels are changed such that $S \rightarrow L$ and $L \rightarrow A$, anti-Stokes scattering is shown instead. Stimulated Stokes (anti-Stokes) Raman scattering is given by adding n to the photon number in the second (first) resonator mode in the upper panel and adding n incoming and outgoing photons to the S (A) mode in the rest of the figure.

laser mode and the other representing the Stokes or anti-Stokes mode. The Hamiltonian of the system is given by Eqs. (15) and (16).

(a) *Stokes Raman scattering.* Setting $\omega_a = \omega_b + \omega_q$, and making the connections $a = L$, $b = S$, and $q = V$, the transition $|1,0,g\rangle \rightarrow |0,1,e\rangle$ emulates Stokes Raman scattering. The virtual transitions involved are shown in Fig. 4. This process is further discussed in the concurrent work of Ref. [55] as a means to achieve single-photon frequency conversion controlled by

the qubit. The effective interaction due to the virtual transitions when $\omega_q \approx \omega_a - \omega_b$ becomes

$$\hat{H}_{\text{int}}^{\text{eff}} = g_{\text{eff}}|1,0,g\rangle\langle 0,1,e| + \text{H.c.} \quad (33)$$

Second-order perturbation theory using Eq. (10) and Fig. 4 gives

$$g_{\text{eff}} = g_a g_b \sin \theta \cos \theta \left(\frac{1}{-\omega_a} - \frac{1}{\Delta_{qa}} + \frac{1}{\omega_b} - \frac{1}{\Omega_{bq}} \right), \quad (34)$$

which reduces to

$$g_{\text{eff}} = g_a g_b \left(\frac{1}{\omega_b} - \frac{1}{\omega_a} \right) \sin(2\theta) \quad (35)$$

on resonance ($\omega_q = \omega_a - \omega_b$). This agrees with the result obtained using adiabatic elimination in Ref. [55].

We also note that it has been shown that a photon scattering off a qubit ultrastrongly coupled to an open transmission line can be down-converted in frequency, leaving some of its energy with the qubit [48]. However, this down-conversion process is not deterministic.

(b) *Anti-Stokes Raman scattering.* The same setup as for Stokes Raman scattering, but considering the reverse transition $|0,1,e\rangle \rightarrow |1,0,g\rangle$, implements anti-Stokes Raman scattering. In this case, we need to make the identifications $a = A$, $b = L$, and $q = V$.

(c) *Stimulated Raman scattering.* We can again consider the same setup, but instead look at the transitions $|1,n,g\rangle \rightarrow |0,n+1,e\rangle$ and $|n,1,e\rangle \rightarrow |n+1,0,g\rangle$ to obtain stimulated Stokes Raman scattering and stimulated anti-Stokes Raman scattering, respectively. In calculating the effective coupling g_{eff} between the initial and final states, as done above and in Ref. [55] for the case $n = 0$, we will, for each possible path between them, multiply the corresponding transition matrix elements. As can be seen from Fig. 4, each path contains exactly one transition that changes the number of excitations in one of the modes from n to $n + 1$. This contributes a factor $\sqrt{n+1}$ to the effective coupling, showing that the presence of the additional photons stimulates the transition.

IV. FOUR-WAVE MIXING

In this section, we treat four-wave mixing, starting as in Sec. III with a general description and then treating special cases, such as degenerate four-wave mixing and hyper-Raman scattering. An overview of these processes is given in Fig. 5. We again provide deterministic analogs for each case. Since there are many similarities to the material presented in Sec. III, the treatment here will be a little more concise. However, compared to Sec. III there are more processes to cover and longer paths of virtual transitions to consider in calculating the effective coupling for those processes.

A. General description

1. Nonlinear optics

Four-wave mixing comes in three types, as illustrated in Fig. 5(a). Type I, with the interaction Hamiltonian

$$\hat{H}_{\text{int}} = g \hat{a}_1 \hat{a}_2 \hat{a}_3^\dagger \hat{a}_4^\dagger + g^* \hat{a}_1^\dagger \hat{a}_2^\dagger \hat{a}_3 \hat{a}_4, \quad (36)$$

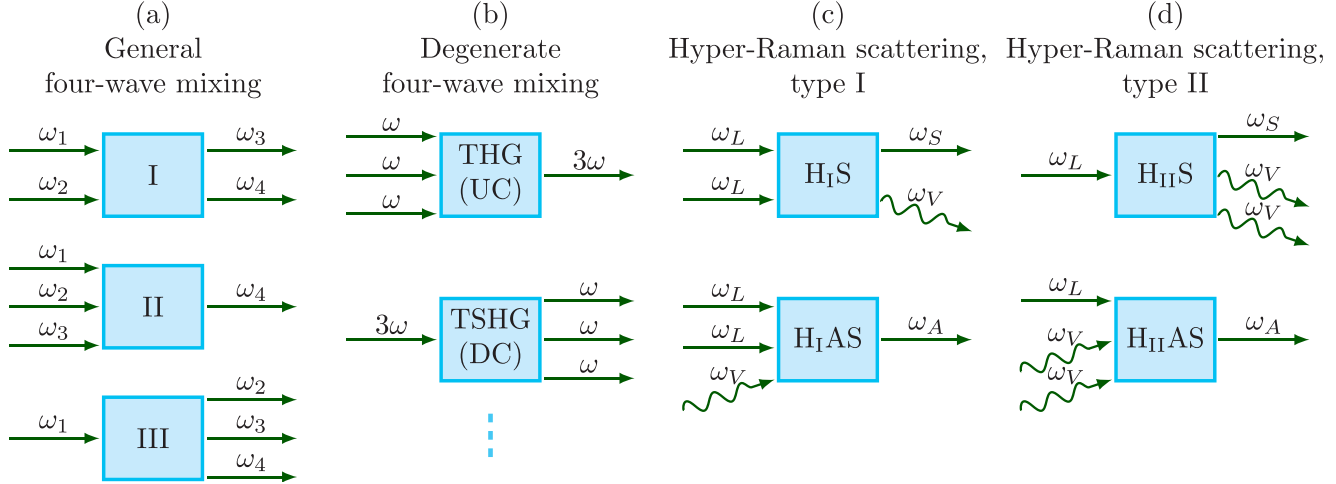


FIG. 5. Schematic representations (Feynman-like diagrams) of four-wave-mixing processes. (a) Four-wave mixing can be divided into three general categories: type I, with two incoming and two outgoing signals (above), type II, with three incoming signals and one outgoing (middle), and type III, with one incoming signal and three outgoing ones (below). (b) When three of the frequencies are degenerate, we have either third-harmonic generation (THG, or up-conversion, above) or third-subharmonic generation (TSHG, or down-conversion, below). When two of the frequencies are degenerate, four processes are possible (not pictured here, but shown in Appendix C). (c) When a phonon is involved, the process is called hyper-Raman scattering of type I. The only change to Stokes (H_{1S} , above) and anti-Stokes (H_{1AS} , below) Raman scattering from the three-wave-mixing case [see Fig. 1(c)] is that there are two (degenerate) incoming photons instead of one. (d) With two degenerate phonons, the process is called hyper-Raman scattering of type II. The two phonons replace the single one in the Stokes (H_{11S} , above) and anti-Stokes (H_{11AS} , below) versions of ordinary Raman scattering from Fig. 1(c).

has two incoming and two outgoing signals. Processes with three incoming signals and one outgoing are here called type II, and processes with one incoming signal and three outgoing ones are here referred to as type III. The interaction Hamiltonian for both types II and III can be written as

$$\hat{H}_{\text{int}} = g \hat{a}_1 \hat{a}_2 \hat{a}_3 \hat{a}_4^\dagger + g^* \hat{a}_1^\dagger \hat{a}_2^\dagger \hat{a}_3^\dagger \hat{a}_4. \quad (37)$$

2. Analogous processes

There are, just as for three-wave mixing, several possible setups that allow deterministic analogs of the four-wave mixing processes. The clearest analogy is probably four resonators all coupled to a single qubit. Adjusting the resonator frequencies to satisfy the condition $\omega_a + \omega_b \approx \omega_c + \omega_d$, the states $|1,1,0,g\rangle$ and $|0,0,1,1,g\rangle$ become resonant and the transitions between these states will constitute type-I four-wave mixing. Similarly, if $\omega_a + \omega_b + \omega_c \approx \omega_d$, the transition $|1,1,1,0,g\rangle \rightarrow |0,1,1,1,g\rangle$ corresponds to type-II mixing and the reverse process $|0,1,1,1,g\rangle \rightarrow |1,0,0,0,g\rangle$ will be type-III mixing.

If at least one of the excitations in the four-wave mixing can be hosted in a qubit, additional setups are possible. With three resonators coupled to a single qubit, $|1,1,0,g\rangle \leftrightarrow |0,0,1,e\rangle$ corresponds to type-I mixing and the processes $|1,1,1,g\rangle \leftrightarrow |0,0,0,e\rangle$ corresponds to type-II (\rightarrow) and type-III (\leftarrow) mixing, respectively. In the same way, with two resonators coupled to two qubits, $|1,1,g,g\rangle \leftrightarrow |0,0,e,e\rangle$ are analogs of type-I mixing and the processes $|0,1,e,e\rangle \leftrightarrow |1,0,g,g\rangle$ are some possible analogs for type-II (\rightarrow) and type-III (\leftarrow) mixing, respectively. Finally, with a single resonator coupled to three qubits, $|1,e,g,g\rangle \leftrightarrow |0,g,e,e\rangle$ corresponds to type-I mixing and the processes $|0,e,e,e\rangle \leftrightarrow |1,g,g,g\rangle$ corresponds to type-II (\rightarrow) and type-III (\leftarrow) mixing, respectively. Hosting at least one

excitation in a qubit may be preferable, since such setups, in general, will require one less intermediate virtual transition than the setup with four resonators and a qubit. Barring destructive interference between the various virtual transition paths, this implies that the effective coupling will be weaker in the latter setup.

All these processes can occur due to intermediate virtual transitions as before. However, in contrast to three-wave mixing, the four-wave mixing analogs do not require the generalized Rabi interaction Hamiltonian from Eq. (6). The standard quantum Rabi model in Eq. (4) is sufficient, since the parity of the number of excitation is conserved in four-wave mixing. In fact, for type-I processes, which do not change the number of excitations, the interaction terms from the JC model in Eq. (5) are sufficient to mediate the required virtual transitions. However, terms from the full quantum Rabi model can still give a significant contribution to the effective coupling between the initial and final states of such processes.

B. Degenerate four-wave mixing: Third-harmonic and third-subharmonic generation

In this subsection, we limit our analysis to the cases where three of the signals involved are degenerate. The cases with two degenerate signals are reviewed briefly in Appendix C.

1. Nonlinear optics

Let us analyze a degenerate case of four-wave mixing assuming $\hat{a}_1 = \hat{a}_2 = \hat{a}_3 \equiv \hat{a}$, $\hat{a}_4 \equiv \hat{a}_+$, and $\omega_+ = 3\omega$. The creation and annihilation of a photon in the Fock basis can be given as $|n, n_+\rangle \rightarrow |n - 3, n_+ + 1\rangle$ for third-harmonic generation (up-conversion) and $|n, n_+\rangle \rightarrow |n + 3, n_+ - 1\rangle$ for third-subharmonic generation (down-conversion); see also

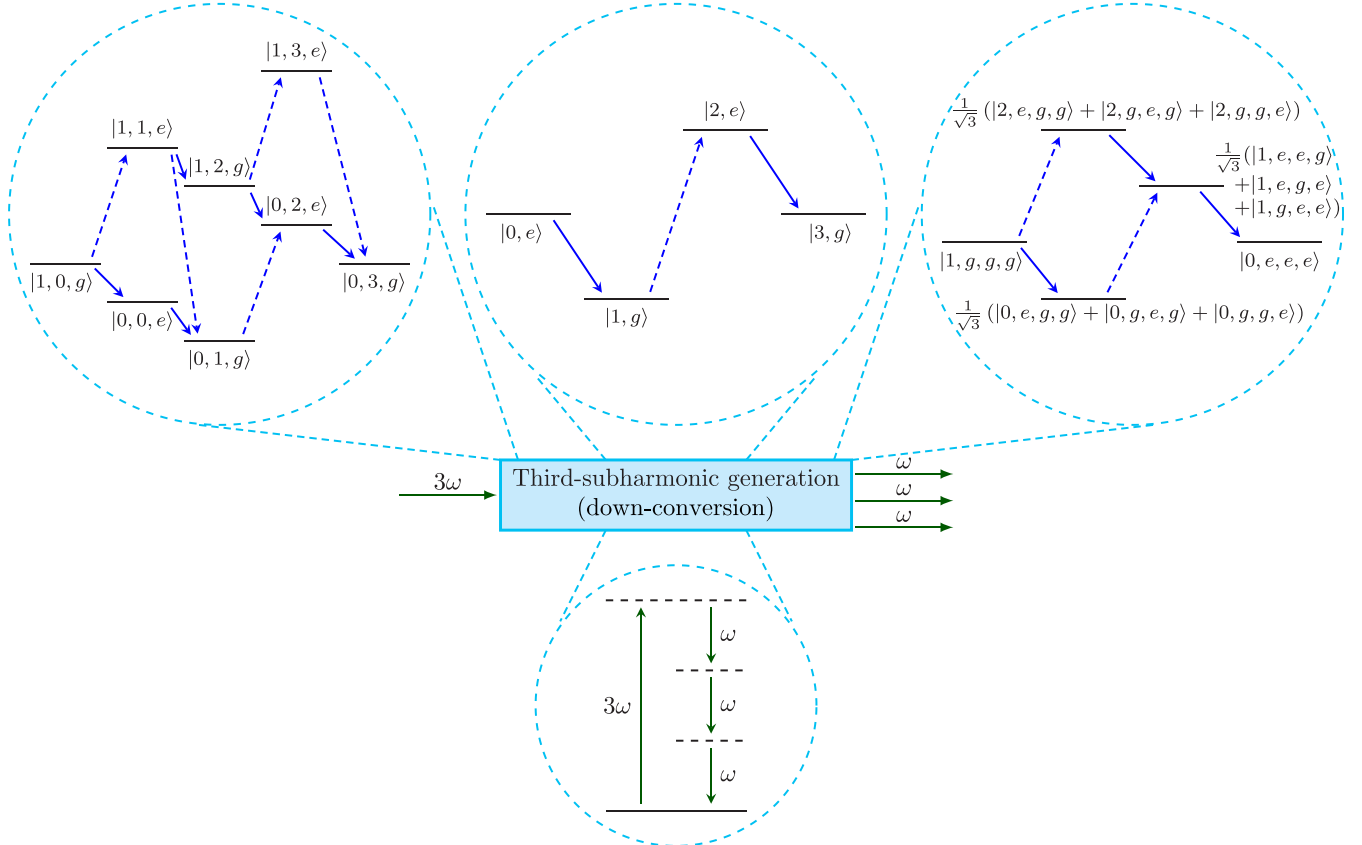


FIG. 6. Realizations of down- and up-conversion with four-wave mixing. The upper left panel shows all virtual transitions that contribute to the down-conversion process (third-subharmonic generation) $|1,0,g\rangle \rightarrow |0,3,g\rangle$ to lowest order. Similarly, the upper middle panel shows all virtual transitions that contribute to the down-conversion process $|0,e\rangle \rightarrow |3,g\rangle$ to lowest order, and the upper right panel shows all virtual transitions that contribute to the down-conversion process $|1,g,g,g\rangle \rightarrow |0,e,e,e\rangle$ to lowest order. The lower panel show the generic level diagram for the process in nonlinear optics. The same arrow and level styles as in Fig. 2 are used. In the upper left panel, $\omega_a = 3\omega_b$ and $\omega_q = 2\omega_b$; in the upper middle panel, we have set $\omega_q = 3\omega_a$; in the upper right panel, $\omega_a = 3\omega_q$. If the directions of all arrows in the entire figure are reversed, up-conversion (third-harmonic generation) is shown instead.

Fig. 5(b). The interaction Hamiltonian for both processes reads

$$\hat{H}_{\text{int}} = g\hat{a}^3\hat{a}_+^\dagger + g^*\hat{a}^{\dagger 3}\hat{a}_+. \quad (38)$$

The initial pure state for third-subharmonic generation is usually chosen as $|\psi(t_0)\rangle = \sum_{n=0}^{\infty} c_n |n,0\rangle$, while that for third-harmonic generation can read as $|\psi(t_0)\rangle = \sum_{n_+=0}^{\infty} c_{n_+} |0,n_+\rangle$, where c_n and c_{n_+} are arbitrary complex amplitudes like in Sec. III B 1.

2. Analogous processes

Also in this case, there are various possible deterministic setups, extensions of those discussed in Sec. III B 2. The three most straightforward setups are illustrated in Fig. 6. We note from the figure that although these setups in general require one more intermediate step than in the three-wave-mixing case, the calculations of the effective coupling are simplified by the fact that we only need to use transitions mediated by the quantum Rabi Hamiltonian (blue arrows in the figure), and not the $\hat{\sigma}_z$ terms of the generalized Rabi Hamiltonian (red arrows in Fig. 2), since the excitation-number parity is conserved.

(a) *Two resonators.* The first analog, shown in the upper left panel of Fig. 6, utilizes two resonators, with frequencies

$\omega_a \approx 3\omega_b$, coupled to a single qubit such that virtual intermediate transitions enable the process $|1,0,g\rangle \leftrightarrow |0,3,g\rangle$, which realizes both up- and down-conversion. The full Hamiltonian for this system is given by Eq. (15) and

$$\hat{H}_{\text{int}} = [g_a(\hat{a} + \hat{a}^\dagger) + g_b(\hat{b} + \hat{b}^\dagger)]\hat{\sigma}_x. \quad (39)$$

We can derive, in the same way as before, an effective Hamiltonian

$$\hat{H}_{\text{int}}^{\text{eff}} = g_{\text{eff}}|1,0,g\rangle\langle 0,3,g| + \text{H.c.} \quad (40)$$

The effective coupling requires fourth-order perturbation theory to calculate. Summing the four contributing paths using Eq. (10) with $|i\rangle = |0,3,g\rangle$ and $|f\rangle = |1,0,g\rangle$ gives

$$\begin{aligned} g_{\text{eff}} = & \sqrt{6}g_a g_b^3 \left[-\frac{1}{(\Omega_{aq} - 2\omega_b)\Delta_{ab}\Omega_{aq}} \right. \\ & + \frac{1}{(\Omega_{aq} - 2\omega_b)\Delta_{ab}\Delta_{bq}} - \frac{1}{2\omega_b(\Omega_{aq} - 2\omega_b)\Delta_{bq}} \\ & \left. + \frac{1}{2\omega_b(3\omega_b + \omega_q)\Delta_{bq}} \right]. \end{aligned} \quad (41)$$

Applying the resonance condition $\omega_a = 3\omega_b$ simplifies this result to

$$\begin{aligned} g_{\text{eff}} &= \frac{\sqrt{6}g_a g_b^3}{2\omega_b} \left[\frac{1}{\Delta_{bq}(3\omega_b - \omega_q)} - \frac{1}{\Omega_{bq}(3\omega_b + \omega_q)} \right] \\ &= \frac{4\sqrt{6}g_a g_b^3 \omega_q}{9\omega_b^4 - 10\omega_b^2 \omega_q^2 + \omega_q^4}, \end{aligned} \quad (42)$$

which scales as $(g_j/\omega)^3$, $j = a, b$, as expected for a fourth-order process.

(b) *Multiphoton Rabi oscillations*. The second option, shown in the upper middle panel of Fig. 6, is multiphoton Rabi oscillations between the states $|0,e\rangle$ and $|3,g\rangle$ with a single resonator coupled to a single qubit ($\omega_q \approx 3\omega_a$), a process studied in Refs. [52,53]. The Hamiltonian for the system is given by Eqs. (3) and (4).

The effective interaction Hamiltonian for this process is

$$\hat{H}_{\text{int}}^{\text{eff}} = g_{\text{eff}}|0,e\rangle\langle 3,g| + \text{H.c.} \quad (43)$$

The effective coupling for three-photon Rabi oscillations follows immediately from third-order perturbation theory as there is only a single path contributing. With $|i\rangle = |3,g\rangle$ and $|f\rangle = |0,e\rangle$, Eq. (10) gives

$$g_{\text{eff}} = \frac{\sqrt{6}g^3}{2\omega_a \Delta_{aq}} = -\frac{9\sqrt{6}g^3}{4\omega_q^2}, \quad (44)$$

where we used the resonance condition $\omega_q = \omega_a/3$ in the last step. This result was also derived in Ref. [52] using adiabatic elimination.

(c) *Three identical qubits*. A third possibility, shown in the upper right panel of Fig. 6, is coupling a single resonator to three identical qubits ($\omega_a = 3\omega_q$), such that the process $|1,g,g,g\rangle \leftrightarrow |0,e,e,e\rangle$ is implemented, as discussed in Ref. [54]. In this case, the Hamiltonian for the system is

$$\hat{H} = \omega_a \hat{a}^\dagger \hat{a} + \sum_{j=1}^3 \omega_q \frac{\hat{\sigma}_z^{(j)}}{2} + \hat{H}_{\text{int}}, \quad (45)$$

$$\hat{H}_{\text{int}} = g(\hat{a} + \hat{a}^\dagger) \sum_{j=1}^3 \hat{\sigma}_x^{(j)}, \quad (46)$$

and the effective interaction Hamiltonian of interest is

$$\hat{H}_{\text{int}}^{\text{eff}} = g_{\text{eff}}|1,g,g,g\rangle\langle 0,e,e,e| + \text{H.c.} \quad (47)$$

The effective coupling can be calculated with third-order perturbation theory. Following Eq. (10), adding up the contributions from the two paths with $|i\rangle = |0,e,e,e\rangle$ and $|f\rangle = |1,g,g,g\rangle$, leads to

$$g_{\text{eff}} = g^3 \left(\frac{3}{\Delta_{qa}^2} + \frac{6}{2\omega_q \Delta_{qa}} \right) = -\frac{3g^3(\omega_a - 3\omega_q)}{\omega_q \Delta_{qa}^2}, \quad (48)$$

which goes to zero on resonance ($\omega_a = 3\omega_q$); the two paths interfere destructively then. However, as shown numerically in the appendix of Ref. [54], a coupling between the states $|1,g,g,g\rangle$ and $|0,e,e,e\rangle$ nevertheless exists close to that resonance. This is partly due to the fact that the energy levels are shifted from their bare-state values to the dressed states

induced by the ultrastrong interaction and partly due to the influence of higher-order processes.

Comparing the three analogs given here, we note that the multiphoton Rabi oscillations and the single photon exciting three qubits both require one less intermediate step than the setup with two resonators and one qubit. However, in the three-qubit case this does not necessarily translate into a stronger effective coupling due to destructive interference between the virtual transitions. The possibility of such destructive interference diminishing the effective coupling needs to be kept in mind when designing analogs of nonlinear optics in these setups. We will see one more example of this phenomenon below.

C. Hyper-Raman scattering, type I: Two-photon processes

1. Nonlinear optics

Hyper-Raman scattering is a generalization of Raman scattering (see Sec. III C) to include either multiple incoming photons or multiple phonons. Here, we first analyze hyper-Raman scattering based on two-photon processes (we refer to this as type-I hyper-Raman scattering), as described by the following Hamiltonians for Stokes frequency,

$$\hat{H}_{\text{int}}^{(S)} = g_S \hat{a}_L^\dagger \hat{a}_S^\dagger \hat{a}_V + \text{H.c.}, \quad (49)$$

and anti-Stokes frequency (which could also be called sideband hypercooling of type I),

$$\hat{H}_{\text{int}}^{(A)} = g_A^* \hat{a}_L^2 \hat{a}_A^\dagger \hat{a}_V + \text{H.c.} \quad (50)$$

These processes are sketched in Fig. 5(c). We note that here $\omega_S > \omega_L$, contrary to the standard Raman scattering case. For simplicity, we have omitted multiphonon versions analogous to Eq. (29).

2. Analogous processes

Just as in Sec. III C 2, we consider setups where qubit excitations play the role of phonons in the deterministic analogs of hyper-Raman scattering. For the type-I process, two resonators (one corresponding to the L mode, one corresponding to the S or A mode) are coupled to a single qubit. This setup is studied further in our concurrent work Ref. [55] as a means to implement deterministic up- and down-conversions controlled by a qubit.

(a) *Stokes Hyper-Raman scattering, type I*. Setting $\omega_a + \omega_q \approx 2\omega_b$ and making the connections $a = S, b = L$, and $q = V$, we see that the process $|0,2,g\rangle \rightarrow |1,0,e\rangle$ corresponds to Stokes hyper-Raman scattering of type I. In the upper panel of Fig. 7, we show the virtual transitions contributing to this process. From the full system Hamiltonian, given by Eqs. (15) and (39) just as for the three-photon frequency conversion in Sec. IV B 2 a, we can derive the effective Hamiltonian

$$\hat{H}_{\text{int},\text{HS}}^{\text{eff}} = g_{\text{eff}}|0,2,g\rangle\langle 1,0,e| + \text{H.c.} \quad (51)$$

Third-order perturbation theory following Eq. (10) gives

$$\begin{aligned} g_{\text{eff}} &= \sqrt{2}g_a g_b^2 \left(\frac{1}{-2\omega_b \Delta_{qb}} + \frac{1}{\Delta_{ab} \Delta_{qb}} + \frac{1}{\Delta_{ab} \Omega_{aq}} \right) \\ &= \frac{\sqrt{2}g_a g_b^2 (\omega_a - 2\omega_b)}{\omega_b \Delta_{ab}^2}, \end{aligned} \quad (52)$$

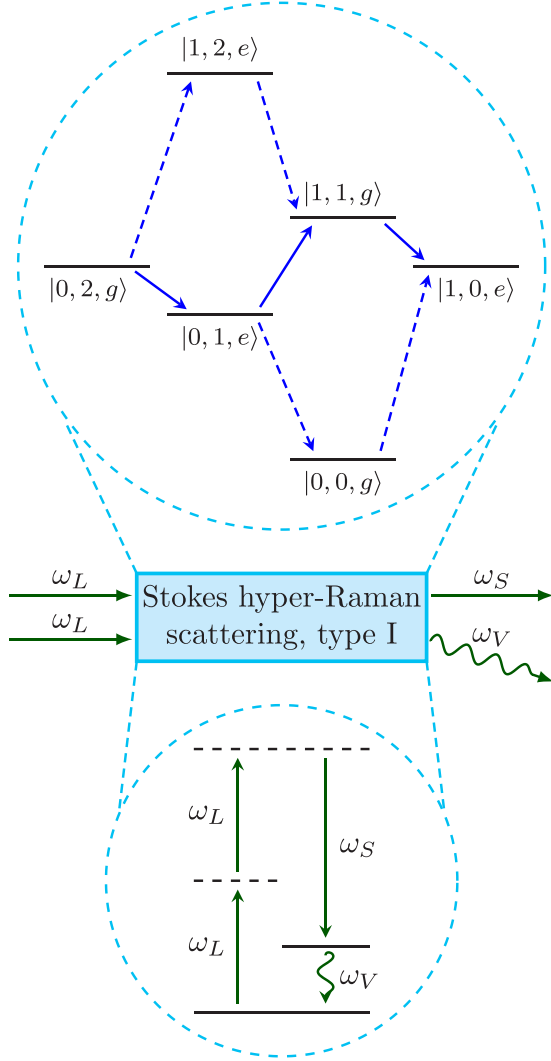


FIG. 7. Stokes hyper-Raman scattering of type I and its deterministic analog. The upper panel shows all virtual transitions that contribute to lowest order to the transition $|0,2,g\rangle \rightarrow |1,0,e\rangle$. The lower panel shows the generic level diagram for the process in nonlinear optics. The connection becomes clear with the identifications $a = S$, $b = L$, and $q = V$. The same arrow and level styles as in Fig. 2 are used; we have set $\omega_a = 3\omega_q$ and $\omega_b = 2\omega_q$.

where we used the resonance condition $\omega_q = 2\omega_b - \omega_a$ in the last step.

We note that one of the paths contributing to the coupling [the second term in Eq. (52)] only requires interactions given by the JC version of the interaction Hamiltonian,

$$\hat{H}_{\text{int}} = g_a(\hat{a}\hat{\sigma}_+ + \hat{a}^\dagger\hat{\sigma}_-) + g_b(\hat{b}\hat{\sigma}_+ + \hat{b}^\dagger\hat{\sigma}_-). \quad (53)$$

Omitting the other terms from Eq. (52) and setting $\omega_q = 2\omega_b - \omega_a$, the result is

$$g_{\text{eff}} = -\frac{\sqrt{2}g_ag_b^2}{\Delta_{ab}^2}. \quad (54)$$

These effective couplings are also calculated in Ref. [55] using adiabatic elimination. In that case, the results are a little more complicated since some higher-order contributions are

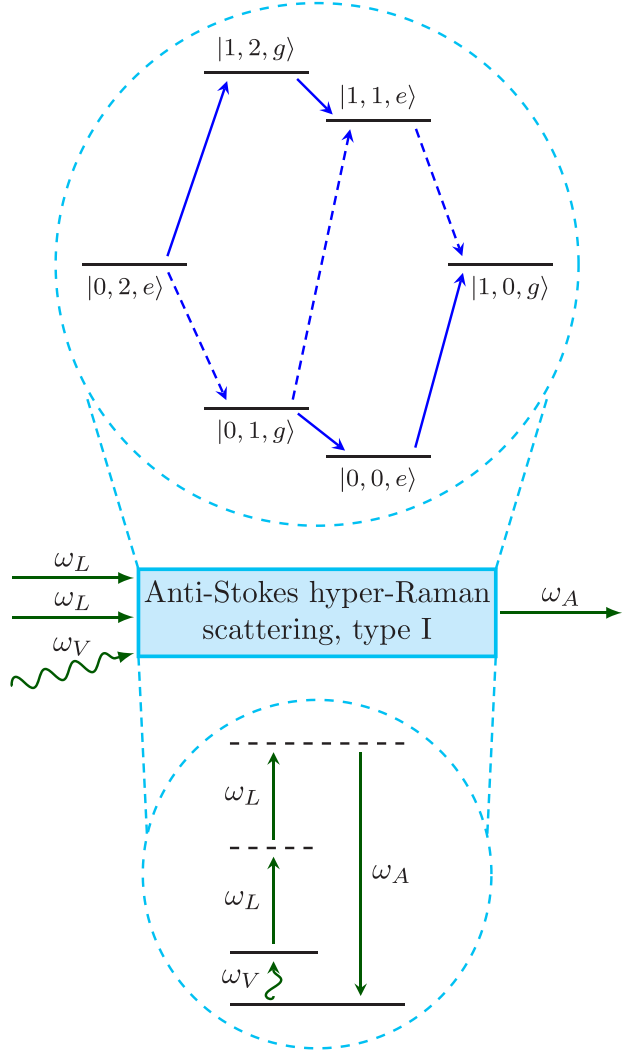


FIG. 8. Anti-Stokes hyper-Raman scattering of type I (sideband hypercooling) and its deterministic analog. The upper panel shows all virtual transitions that contribute to lowest order to the transition $|0,2,e\rangle \rightarrow |1,0,g\rangle$. The lower panel shows the generic level diagram for the process in nonlinear optics. The connection becomes clear with the identifications $a = A$, $b = L$, and $q = V$. The same arrow and level styles as in Fig. 2 are used; we have set $\omega_a = 5\omega_q$ and $\omega_b = 2\omega_q$.

included, but to lowest order the results coincide with those given here.

(b) *Anti-Stokes Hyper-Raman scattering, type I.* If we instead set $\omega_a \approx 2\omega_b + \omega_q$ in the same setup as for Stokes hyper-Raman scattering of type I (and make the connections $a = A$, $b = L$, and $q = V$), the transition $|0,2,e\rangle \rightarrow |1,0,g\rangle$ corresponds to anti-Stokes hyper-Raman scattering of type I. The effective interaction Hamiltonian becomes

$$\hat{H}_{\text{int},\text{HiAS}}^{\text{eff}} = g_{\text{eff}}|0,2,e\rangle\langle 1,0,g| + \text{H.c.} \quad (55)$$

The virtual transitions contributing to the process $|0,2,e\rangle \rightarrow |1,0,g\rangle$ are shown in Fig. 8. Third-order perturbation theory

following Eq. (10) gives

$$\begin{aligned} g_{\text{eff}} &= \sqrt{2}g_a g_b^2 \left(\frac{1}{2\omega_b \Omega_{qb}} - \frac{1}{\Delta_{ab} \Omega_{qb}} + \frac{1}{\Delta_{ab} \Delta_{aq}} \right) \\ &= \frac{\sqrt{2}g_a g_b^2 (\omega_a - 2\omega_b)}{\omega_b \Delta_{ab}^2}, \end{aligned} \quad (56)$$

where we used the resonance condition $\omega_q = \omega_a - 2\omega_b$ in the last step. We note that the expression is the same as the one obtained for type-I Stokes hyper-Raman scattering in Eq. (52), despite the resonance condition being different.

This effective coupling is also calculated in Ref. [55] using adiabatic elimination. Again, in that case, the result is a little more complicated since some higher-order contributions are included, but to lowest order it coincides with Eq. (56).

D. Hyper-Raman scattering, type II: Two-phonon processes

1. Nonlinear optics

Hyper-Raman scattering can also be based on two-phonon processes (we refer to this as type-II hyper-Raman scattering), as described by the following interaction Hamiltonians with Stokes frequency,

$$\hat{H}_{\text{int}}^{(S)} = g_S \hat{a}_L \hat{a}_S^\dagger \hat{a}_{V1}^\dagger \hat{a}_{V2}^\dagger + \text{H.c.}, \quad (57)$$

and with anti-Stokes frequency (which could also be called sideband hypercooling of type II),

$$\hat{H}_{\text{int}}^{(A)} = g_A^* \hat{a}_L \hat{a}_A^\dagger \hat{a}_{V1} \hat{a}_{V2} + \text{H.c.} \quad (58)$$

These processes are sketched in Fig. 5(d).

2. Analogous processes

The closest analog here is a setup with two resonators both coupled to two identical qubits. The full system Hamiltonian is given by

$$\hat{H} = \omega_a \hat{a}^\dagger \hat{a} + \omega_b \hat{b}^\dagger \hat{b} + \sum_{j=1}^2 \omega_q \frac{\hat{\sigma}_z^{(j)}}{2} + \hat{H}_{\text{int}}, \quad (59)$$

$$\hat{H}_{\text{int}} = [g_a(\hat{a} + \hat{a}^\dagger) + g_b(\hat{b} + \hat{b}^\dagger)] \sum_{j=1}^2 \hat{\sigma}_x^{(j)}. \quad (60)$$

If the frequencies satisfy the resonance condition $\omega_a \approx \omega_b + 2\omega_q$, the process $|1,0,g,g\rangle \rightarrow |0,1,e,e\rangle$, whose virtual transitions are shown in Fig. 9, corresponds to Stokes hyper-Raman scattering of type II, given that we make the connections $a = L$, $b = S$, and $q = V$. The reverse process corresponds to anti-Stokes hyper-Raman scattering of type II, if we instead identify $a = A$ and $b = L$.

The virtual transitions give rise to the effective Hamiltonian

$$\hat{H}_{\text{int}}^{\text{eff}} = g_{\text{eff}} |1,0,g,g\rangle \langle 0,1,e,e| + \text{H.c.}, \quad (61)$$

which describes both processes. Adding up the two paths in Fig. 9 using second-order perturbation theory following Eq. (10), we obtain

$$g_{\text{eff}} = 2g_a g_b \left(\frac{1}{\Delta_{qa}} + \frac{1}{\Omega_{bq}} \right) = -\frac{2g_a g_b (\Delta_{ba} + 2\omega_q)}{\Delta_{aq} \Omega_{bq}}, \quad (62)$$

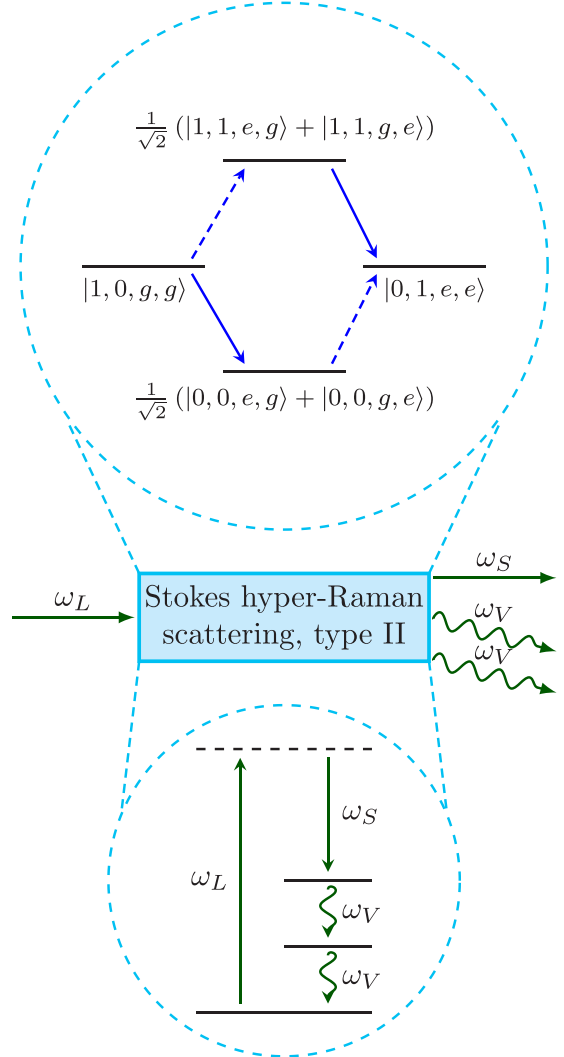


FIG. 9. Stokes hyper-Raman scattering of type II and its deterministic analog. The upper panel shows all virtual transitions that contribute to lowest order to the transition $|1,0,g,g\rangle \rightarrow |0,1,e,e\rangle$. The lower panel shows the generic level diagram for the process in nonlinear optics. The connection becomes clear with the identifications $a = L$, $b = S$, and $q = V$. The same arrow and level styles as in Fig. 2 are used; we have set $\omega_a = 2\omega_b = 4\omega_q$. If the directions of all arrows in the entire figure are reversed, and the labels are changed such that $S \rightarrow L$ and $L \rightarrow A$, anti-Stokes hyper-Raman scattering of type II is shown instead.

which goes to zero on resonance ($\omega_a = \omega_b + 2\omega_q$). However, a finite coupling should result from the fact that bare energy levels are shifted to dressed ones and higher-order processes can contribute, analogous to the situation for the single photon exciting three qubits discussed in Sec. IV B 2 c.

V. OTHER NONLINEAR PROCESSES

While three- and four-wave mixing have been the main focus of this article, there are several other nonlinear-optics processes for which analogs can be found. In this section, we treat a few of these.

A. Higher-harmonic and -subharmonic generation

A plethora of processes are possible when considering wave-mixing involving five or more frequencies. To shed light on the relevant considerations for the deterministic analogs of these processes, it is sufficient to consider higher-harmonic and -subharmonic generation as a simple representative example.

1. Nonlinear optics

We consider the degenerate case of m -wave mixing assuming $\hat{a}_1 = \hat{a}_2 = \dots = \hat{a}_{m-1} \equiv \hat{a}$, $\hat{a}_m \equiv \hat{a}_+$, and $\omega_+ = (m-1)\omega$. The creation and annihilation of a photon in the Fock basis can then be given as $|n, n_+\rangle \rightarrow |n-m+1, n_+ + 1\rangle$ for $(m-1)$ th-harmonic generation (up-conversion) and $|n, n_+\rangle \rightarrow |n+m-1, n_+ - 1\rangle$ for $(m-1)$ th-subharmonic generation (down-conversion). The interaction Hamiltonian for both processes can be written as

$$\hat{H}_{\text{int}} = g\hat{a}^{m-1}\hat{a}_+^\dagger + g^*\hat{a}^{\dagger(m-1)}\hat{a}_+, \quad (63)$$

generalizing Eq. (14) for three-wave mixing and Eq. (38) for four-wave mixing.

2. Analogous processes

It is straightforward to extend the three approaches discussed in Sec. III B 2 for three-wave mixing and in Sec. IV B 2 for four-wave mixing. One can use two resonators, with frequencies $\omega_a = (m-1)\omega_b$, coupled to a single qubit such that the process $|1, 0, g\rangle \leftrightarrow |0, m-1, g\rangle$ is enabled by virtual intermediate transitions, realizing both up- and down-conversion. The other approaches are to use multiphoton Rabi oscillations between $|0, e\rangle$ and $|m-1, g\rangle$ using a single resonator coupled to a single qubit with $\omega_q = (m-1)\omega_a$ [53]; or to couple a single resonator to $m-1$ identical qubits [$\omega_a = (m-1)\omega_q$] such that the process $|1, g, \dots, g\rangle \leftrightarrow |0, e, \dots, e\rangle$ is realized [54].

What these three approaches, and all other analogs of m -wave mixing, have in common are that they require an increasing number of intermediate virtual transitions as m increases. In general, the effective coupling g_{eff} , determining the transition rate, will be proportional to $(g/\omega)^{n-1}$ if n steps of intermediate virtual transitions are required to go between the initial and final states. Here, g and ω are the coupling and the relevant system frequencies, respectively, in the quantum Rabi model discussed in Sec. II B. Considering this, the fact that the multiphoton Rabi oscillations require one less intermediate step than the other two approaches described above (see Secs. III B 2 and IV B 2) makes them the most suited to implement an analog of higher-harmonic and -subharmonic generation.

We also note that the standard quantum Rabi model, Eq. (4), is sufficient to mediate the virtual transitions needed for m -wave mixing when m is even. If m is odd, the interaction terms from the generalized quantum Rabi model, Eq. (6), are necessary to realize the analogs discussed here.

B. Multiphoton absorption

1. Nonlinear optics

Simultaneous absorption of multiple photons in a system is a nonlinear process, first predicted by Göppert-Mayer [69]. Unlike most of the wave-mixing processes discussed above

(except Raman scattering), this process changes the net energy of the system.

2. Analogous processes

A clear analogy of multiphoton absorption is provided by the multiphoton Rabi oscillations [53] already discussed in the context of harmonic and subharmonic generation in Secs. III B 2, IV B 2, and VA 2. During a multiphoton Rabi oscillation, a single qubit absorbs n photons from the resonator it is coupled to; this is the process $|n, g\rangle \rightarrow |0, e\rangle$. We also note that circuit-QED experiments with flux qubits have demonstrated multiphoton absorption in a driven qubit-resonator system [32,63].

C. Parametric processes

1. Nonlinear optics

Many of the processes discussed above can be analyzed for the case where one of the fields is a strong drive that can be approximated as classical. As an example, consider the general three-wave-mixing processes described by Eqs. (11) and (12) in Sec. III A 1. We denote the frequencies by $\omega_p \equiv \omega_1$ for the pump (drive) mode, $\omega_s \equiv \omega_2$ for the signal mode, and $\omega_i \equiv \omega_\pm$ for the idler mode. We then apply the parametric approximation $\hat{a}_p(t) \approx \langle \hat{a}_p(t) \rangle \approx \alpha_p(t) \equiv |\alpha_p| \exp[-i(\omega t + \phi_p)]$, which is usually valid if $\langle \hat{n}_p(t) \rangle \approx \langle \hat{n}_p(t_0) \rangle \gg \max\{1, \langle \hat{n}_s(t) \rangle, \langle \hat{n}_i(t) \rangle\}$, where \hat{n}_x is the number of photons in mode x . For the case $\omega_p = \omega_s + \omega_i$, Eq. (12) then becomes

$$\begin{aligned} \hat{H}^{(\text{amp})} &= g^* \alpha_p^* \hat{a}_i \hat{a}_s + g \alpha_p \hat{a}_i^\dagger \hat{a}_s^\dagger \\ &= \kappa [\hat{a}_i \hat{a}_s e^{i(\omega t + \phi)} + \hat{a}_i^\dagger \hat{a}_s^\dagger e^{-i(\omega t + \phi)}], \end{aligned} \quad (64)$$

where $\omega \equiv \omega_p$, the coupling constant g is rescaled as $\kappa = |g\alpha_p|$, and $\phi = \phi_p - \arg(g)$. This equation describes parametric amplification (down-conversion). For the special case $\omega_s = \omega_i$, it corresponds to degenerate parametric down-conversion. Similarly, under the parametric approximation, with $\hat{a}_1 \equiv \hat{a}_p \approx \alpha_p$, Eq. (11) describes parametric frequency conversion.

2. Analogous processes

As discussed in Sec. III B 2 a, Ref. [65] showed that a setup with two resonator modes coupled to a qubit with the interaction of Eq. (6) can give an effective interaction of the form

$$\hat{H}_{\text{int}}^{\text{eff}} = \zeta (\hat{a}^{\dagger 2} \hat{b} + \hat{a}^2 \hat{b}^\dagger) \hat{\sigma}_z, \quad (65)$$

where

$$\zeta = \frac{g_a^2 g_b^2 \sin \theta \sin(2\theta)}{\omega_a(\omega_q - \omega_b)}. \quad (66)$$

This interaction results in degenerate parametric down-conversion and squeezing. Note that the qubit state will affect the process since the interaction is proportional to $\hat{\sigma}_z$, which is absent in Eq. (64). However, if we assume that the qubit remains in its ground (or excited) state during the system evolution, we can recover Eq. (64) from Eq. (65). Such qubit “freezing” can be achieved, e.g., by Zeno-type effects.

In general, similar effective interaction Hamiltonians should be possible to derive for all setups considered in this article where the initial and final states for the system have the same qubit state. Thus, most parametric processes from nonlinear optics have deterministic analogs involving virtual photons.

D. Kerr, cross-Kerr, and Pockels effects

1. Nonlinear optics

The Kerr, cross-Kerr, and Pockels effects differ from the other nonlinear-optics phenomena discussed so far in that they do not involve any change in the number of excitations in some mode. Instead, the frequency of a mode a is modified, either through self-interaction (Kerr effect) or through interaction with a second mode b (Pockels effect when the change is proportional to the amplitude of the field; cross-Kerr effect when the change is proportional to the square of said amplitude). These effects can be described by the following Hamiltonians:

$$\hat{H}_K = \chi_K (\hat{a}^\dagger \hat{a})^2, \quad (67)$$

$$\hat{H}_{cK} = \chi_{cK} \hat{a}^\dagger \hat{a} \hat{b}^\dagger \hat{b}, \quad (68)$$

$$\hat{H}_P = \chi_P \hat{a}^\dagger \hat{a} (\hat{b} + \hat{b}^\dagger), \quad (69)$$

where χ_x gives the strength of the nonlinear interaction.

2. Analogous processes

The Kerr effect can be realized with a single qubit coupled to a resonator with only the JC interaction of Eq. (5). In the dispersive regime, where $g \ll |\omega_a - \omega_q|$, a perturbation expansion in the small parameter $g/(\omega_a - \omega_q)$ yields a term [70]

$$\hat{H}_K^{\text{disp}} = \chi_K (\hat{a}^\dagger \hat{a})^2 \hat{\sigma}_z, \quad (70)$$

where

$$\chi_K = -\frac{g^4}{(\omega_a - \omega_q)^3}. \quad (71)$$

This Hamiltonian reduces to the standard Kerr Hamiltonian, given in Eq. (67), if we can assume that the qubit remains in one and the same state during the system evolution, as discussed above in Sec. V C 2. More general derivations for multiple resonator modes and a multilevel atom in the dispersive regime have shown how both Kerr and cross-Kerr effects can be realized [71,72]. In particular, Ref. [72] demonstrates clearly how an atom coupled to two resonators in the dispersive regime via a general coupling like Eq. (6) gives rise to the Kerr and cross-Kerr effects due to fourth-order processes involving virtual photons in the same way as all other analogs of nonlinear optics discussed previously in this article. We note that these Kerr and cross-Kerr terms, just like in Eqs. (65) and (70), involve sums over the diagonal qubit operators $|g\rangle\langle g|$ and $|e\rangle\langle e|$.

Based on the above theory, experiments in circuit QED have recently demonstrated both the single-photon Kerr [73] and cross-Kerr effects [74]. A large cross-Kerr effect for propagating photons interacting with a three-level artificial atom in circuit QED has also been studied theoretically [75] and experimentally [76]. However, to the best of our

knowledge, no such experimental demonstrations exists for the Pockels effect and we have been unable to find a mechanism for engineering it in the setups we consider.

VI. EXPERIMENTAL FEASIBILITY

In this section, we evaluate the experimental feasibility of our proposed analogs of nonlinear-optics processes. In most of these analogs, the process consists of transferring population from an initial state $|i\rangle$ to a final state $|f\rangle$. The time scale for this process is given by the inverse of the effective coupling strength g_{eff} for the interaction that connects the two states [see Eq. (9)]. For the transfer to be successful, g_{eff} must exceed the relevant decoherence rates in the system: qubit decoherence (relaxation and dephasing) at a rate γ and resonator losses at a rate κ . To observe energy-level anticrossings in spectroscopy, revealing the effective coupling between $|i\rangle$ and $|f\rangle$, it is sufficient that $g_{\text{eff}} > \kappa, \gamma$; for the transfer to be essentially deterministic, i.e., have close to unit efficiency, $g_{\text{eff}} \gg \kappa, \gamma$ is required. Note that when either $|i\rangle$ or $|f\rangle$ contain multiple excitations, the relevant loss rates that g_{eff} should be compared to are the total loss rates for those states. For example, in the case of n th-subharmonic generation through multiphoton Rabi oscillations with $|i\rangle = |0, e\rangle$ and $|f\rangle = |n, g\rangle$, discussed in Sec. V A 2, the effective coupling must be compared to γ and $n\kappa$.

Although USC has been realized in several solid-state systems, as noted in Sec. I, we limit the discussion here to circuit QED, where we believe the proposed experiments are easiest to implement. The experimental demonstrations of USC with qubits coupled to resonators in circuit QED have all used flux qubits, coupled either to lumped-element LC oscillators [19,31,36] or transmission-line resonators [20,29,32]. In such circuit QED experiments, qubit and resonator frequencies are usually in the range $\omega_q, \omega_a \sim 2\pi \times 1\text{--}10\text{ GHz}$. Recent experimental work on flux qubits has demonstrated γ on the order of $2\pi \times 10\text{ kHz}$ [77,78], and an improvement of the flux qubit design [79], which comes at the price of reduced anharmonicity, has been shown to reduce γ even further [80]. Superconducting transmon qubits, which have lower anharmonicity than flux qubits, can have γ approaching $2\pi \times 1\text{ kHz}$ [81,82]. For transmission-line resonators, quality factors $Q = \omega_a/\kappa$ on the order of 10^6 have been demonstrated [83]. Recently, superconducting qubits are often coupled to 3D cavities, where the quality factor can be another two orders of magnitude larger [84].

Taken together, the numbers above indicate that $\gamma, \kappa \sim 10^{-6}\omega_a$ can be reached in state-of-the-art circuit-QED experiments. Regarding the coupling strength, Refs. [19,20,29,32] have reached $g \gtrsim 0.1\omega_a$ and Refs. [31,36] demonstrated $g \sim \omega_a$. Using the lower of these values as a very conservative estimate, we calculate most of the effective coupling strengths derived in Secs. III and IV. The results are given in Table I. We see that even with this conservative estimate for the bare coupling, and even though processes up to fourth order are considered, the effective coupling strengths are orders of magnitude larger than the decoherence rates that have been demonstrated in experiments. If such low decoherence rates would be hard to reach, the effective coupling can instead be much strengthened by a modest increase of the bare coupling.

We note that already one of the first circuit QED experiments to reach the USC regime, Ref. [20], achieved

TABLE I. Conservative estimates of the effective coupling strengths g_{eff} for most of the analogs of three- and four-wave mixing processes given in this article. In each case, we have assumed the bare coupling g to be 10% of the lowest transition frequency in the setup. The effective coupling is given in units of that transition frequency. We note that the parameter θ can be chosen quite freely in experiments with flux qubits.

Process	Parameters	Equation	Effective coupling $ g_{\text{eff}} $
$ 1,0,g\rangle \leftrightarrow 0,2,g\rangle$	$\omega_a = 2\omega_b, \omega_q = 1.5\omega_b, g_{a/b} = 0.1\omega_b, \theta = \pi/6$	Eq. (21)	$3 \times 10^{-3}\omega_b$
$ 0,e\rangle \leftrightarrow 2,g\rangle$	$\omega_q = 2\omega_a, g = 0.1\omega_a, \theta = \pi/4$	Eq. (24)	$1 \times 10^{-2}\omega_a$
$ 1,g,g\rangle \leftrightarrow 0,e,e\rangle$	$\omega_a = 2\omega_q, g = 0.1\omega_q, \theta = \pi/6$	Eq. (28)	$1 \times 10^{-3}\omega_q$
$ 1,0,g\rangle \leftrightarrow 0,1,e\rangle$	$\omega_a = 3\omega_q, \omega_b = 2\omega_q, g_{a/b} = 0.1\omega_q, \theta = \pi/4$	Eq. (35)	$2 \times 10^{-3}\omega_q$
$ 1,0,g\rangle \leftrightarrow 0,3,g\rangle$	$\omega_a = 3\omega_b, \omega_q = 2\omega_b, g_{a/b} = 0.1\omega_b$	Eq. (42)	$1 \times 10^{-4}\omega_b$
$ 0,e\rangle \leftrightarrow 3,g\rangle$	$\omega_q = 3\omega_a, g = 0.1\omega_a$	Eq. (44)	$6 \times 10^{-4}\omega_a$
$ 0,2,g\rangle \leftrightarrow 1,0,e\rangle$	$\omega_a = 3\omega_q, \omega_b = 2\omega_q, g_{a/b} = 0.1\omega_q$	Eq. (52)	$7 \times 10^{-4}\omega_q$
$ 0,2,e\rangle \leftrightarrow 1,0,g\rangle$	$\omega_a = 5\omega_q, \omega_b = 2\omega_q, g_{a/b} = 0.1\omega_q$	Eq. (56)	$2 \times 10^{-4}\omega_q$

sufficiently small decoherence to clearly observe an energy-level anticrossing due to effective coupling between states $|1,0,g\rangle$ and $|0,1,e\rangle$. Furthermore, as noted in Sec. V D 2, the single-photon Kerr and cross-Kerr effects, even though these are fourth-order processes, have also been experimentally demonstrated in circuit QED using transmon qubits and 3D cavities [73,74]. In the case of the Kerr effect, the Kerr coefficient was $\chi_K = 2\pi \times 325$ kHz, much larger than $\gamma, \kappa \sim 2\pi \times 10\text{--}20$ kHz [73].

From the estimates in this section, we conclude that most, if not all, of the nonlinear-optics analogs proposed in this article can be implemented with existing experimental technology in circuit QED. It appears that the effective coupling strengths can be orders of magnitude larger than the system decoherence rates, ensuring that the relevant processes can reach close to unit efficiency.

VII. SUMMARY AND OUTLOOK

We have shown how analogs of nonlinear optics can be realized in systems where one or more qubits are coupled to one or more resonator modes. These analogous processes are all based on the light-matter interaction between a qubit and a photonic mode described by the quantum Rabi Hamiltonian or some generalized version thereof. This interaction allows the number of excitations in the system to change, which makes possible the creation and annihilation of virtual photons and qubit excitations. In this way, initial and final states of the nonlinear-optics processes can be connected via a number of virtual transitions, creating an effective deterministic coupling between the states. The effective coupling decreases when the number of intermediate transition steps increases. However, with the recent experimental demonstrations of USC in a variety of systems, circuit QED in particular, it should now be possible to observe many of these nonlinear-optics phenomena in new settings. When the light-matter coupling becomes ultrastrong, even the weaker effective coupling can be larger than the relevant decoherence rates in the system.

For the case of three-wave mixing, we have shown how analogs can be constructed for sum- and difference-frequency

generation, including the special cases of second-harmonic generation (up-conversion) and second-subharmonic generation (down-conversion) as well as Stokes and anti-Stokes spontaneous and stimulated Raman scattering. A summary of all the three-wave-mixing processes and their analogs is given in Table II.

Similarly, for the case of four-wave mixing, we have shown how analogs can be realized for all types of nondegenerate and degenerate mixing, including third-harmonic and third-subharmonic generation as well as all forms of hyper-Raman scattering. We provide a summary of all the four-wave-mixing processes and their analogs in Table III. Finally, we have also shown that analogs working according to the same principle are available for higher-harmonic and -subharmonic generation, multiphoton absorption, parametric processes, and the Kerr and cross-Kerr effects.

It is noteworthy that some of the setups we consider, especially the relatively simple setups of a single qubit coupled to one or two resonators, can be used to realize many analogs of nonlinear-optics phenomena in one universal system. It is also remarkable that these analogs work at unit efficiency with a minimal number of photons without any need for external drives, which is not the case for conventional nonlinear optics. While some processes that we discuss here have been investigated in previous and concurrent publications, we have now provided a unified and clear picture of how and why nonlinear-optics analogs can be constructed in these setups. One important difference to conventional nonlinear optics is that we are able to suppress lower-order processes by making the final state of such processes far off-resonant with the initial state.

There are many directions for future work following this article. They include deriving effective Hamiltonians for more parametric processes based on the setups discussed here and finding an analog of the Pockels effect. An interesting way to take the ideas of the current work one step further is to consider analogs of nonlinear-optics processes where the excitations are exchanged only between atoms and any resonators in the setups are only excited virtually, which is treated in a concurrent publication [56]. We also see a great potential for using the

TABLE II. A summary of three-wave-mixing processes in nonlinear optics and their deterministic analogs with single atoms and virtual photons. In the case of nondegenerate three-wave mixing, with the exception of Raman scattering, the given frequencies and transitions are just some of the possibilities.

Nonlinear-optics process		Analogous setup	Frequencies	Transition	Hamiltonian	Reference
Degenerate three-wave mixing	Second-harmonic generation (upconversion)	1 resonator, 1 qubit 2 resonators, 1 qubit	$\omega_q = 2\omega_a$ $\omega_a = 2\omega_b$	$ 2, g\rangle \rightarrow 0, e\rangle$ $ 0, 2, g\rangle \rightarrow 1, 0, g\rangle$	Gen. Rabi	Sec. III B, [53]
	1 resonator, 2 qubits	$\omega_a = 2\omega_q$	$ 0, e, e\rangle \rightarrow 1, g, g\rangle$	Gen. Rabi	Sec. III B, [65]	
	1 resonator, 1 qubit	$\omega_q = 2\omega_a$	$ 0, e\rangle \rightarrow 2, g\rangle$	Gen. Rabi	Sec. III B, [54]	
	2 resonators, 1 qubit	$\omega_a = 2\omega_b$	$ 1, 0, g\rangle \rightarrow 0, 2, g\rangle$	Gen. Rabi	Sec. III B, [53]	
	1 resonator, 2 qubits	$\omega_a = 2\omega_q$	$ 1, g, g\rangle \rightarrow 0, e, e\rangle$	Gen. Rabi	Sec. III B, [65]	
	Spontaneous Raman scattering	Stokes		$ 1, 0, g\rangle \rightarrow 0, 1, e\rangle$	Gen. Rabi	Sec. III B, [54]
	Stimulated Raman scattering	anti-Stokes		$ 0, 1, e\rangle \rightarrow 1, 0, g\rangle$	Gen. Rabi	Sec. III C, [55]
	Sum-frequency generation	Stokes	$\omega_a = \omega_b + \omega_q$	$ 1, n, g\rangle \rightarrow 0, n+1, e\rangle$	Gen. Rabi	Sec. III C, [55]
	Difference-frequency generation	anti-Stokes		$ n, 1, e\rangle \rightarrow n+1, 0, g\rangle$	Gen. Rabi	Sec. III C
Non-degenerate three-wave mixing	1 resonator, 2 qubits	$\omega_a = \omega_{q1} + \omega_{q2}$		Gen. Rabi	Sec. III C	
	2 resonators, 1 qubit	$\omega_a + \omega_b = \omega_q$	$ 0, e, e\rangle \rightarrow 1, g, g\rangle$	Gen. Rabi	Sec. III A, [54]	
	3 resonators, 1 qubit	$\omega_a + \omega_b = \omega_c$	$ 1, 1, g\rangle \rightarrow 0, 0, e\rangle$	Gen. Rabi	Sec. III A	
	1 resonator, 2 qubits	$\omega_a = \omega_{q1} + \omega_{q2}$	$ 1, 1, 0, g\rangle \rightarrow 0, 0, 1, g\rangle$	Gen. Rabi	Sec. III A	
	2 resonators, 1 qubit	$\omega_a + \omega_b = \omega_q$	$ 1, g, g\rangle \rightarrow 0, e, e\rangle$	Gen. Rabi	Sec. III A, [54]	
	3 resonators, 1 qubit	$\omega_a + \omega_b = \omega_c$	$ 0, 0, e\rangle \rightarrow 1, 1, g\rangle$	Gen. Rabi	Sec. III A	

TABLE III. A summary of four-wave-mixing processes in nonlinear optics and their deterministic analogs with single atoms and virtual photons. In the case of nondegenerate four-wave mixing, the given frequencies and transitions are just some of the possibilities. For degenerate four-wave mixing with two degenerate signals, see Appendix C.

Nonlinear-optics process		Analogous setup	Frequencies	Transition	Hamiltonian	Reference
Degenerate four-wave mixing	Third-harmonic generation (upconversion)	1 resonator, 1 qubit	$\omega_q = 3\omega_a$	$ 3, g\rangle \rightarrow 0, e\rangle$	Rabi	Sec. IV B, [52, 53]
		2 resonators, 1 qubit	$\omega_a = 3\omega_b$	$ 0, 3, g\rangle \rightarrow 1, 0, g\rangle$	Rabi	Sec. IV B
	Third-subharmonic generation (downconversion)	1 resonator, 3 qubits	$\omega_a = 3\omega_q$	$ 0, e, e, e\rangle \rightarrow 1, g, g, g\rangle$	Rabi	Sec. IV B, [54]
		2 resonators, 1 qubit	$\omega_q = 3\omega_a$	$ 0, e\rangle \rightarrow 3, g\rangle$	Rabi	Sec. IV B, [52, 53]
	Hyper-Raman scattering, type I	1 resonator, 3 qubits	$\omega_a = 3\omega_b$	$ 1, 0, g\rangle \rightarrow 0, 3, g\rangle$	Rabi	Sec. IV B
		2 resonators, 1 qubit	$\omega_a = 3\omega_q$	$ 1, g, g, g\rangle \rightarrow 0, e, e, e\rangle$	Rabi	Sec. IV B, [54]
	Hyper-Raman scattering, type II	Stokes	$\omega_a + \omega_q = 2\omega_b$	$ 0, 2, g\rangle \rightarrow 1, 0, e\rangle$	JC	Sec. IV C, [55]
		anti-Stokes	$\omega_a = 2\omega_b + \omega_q$	$ 0, 2, e\rangle \rightarrow 1, 0, g\rangle$	Rabi	Sec. IV C, [55]
	Type I (2 inputs, 2 outputs)	2 resonators, 2 qubits	$\omega_a = \omega_b + 2\omega_q$	$ 1, 0, g, g\rangle \rightarrow 0, 1, e, e\rangle$	Rabi	Sec. IV D
		3 resonators, 1 qubit	$\omega_a + \omega_b = \omega_c + \omega_q$	$ 0, 1, e, e\rangle \rightarrow 1, 0, g, g\rangle$	Rabi	Sec. IV D
		4 resonators, 1 qubit	$\omega_a + \omega_b = \omega_c + \omega_d$	$ 1, 1, 0, g\rangle \rightarrow 0, 0, 1, e\rangle$	JC	Sec. IV A
		2 resonators, 2 qubits	$\omega_a + \omega_b = \omega_{q1} + \omega_{q2}$	$ 1, 1, g, g\rangle \rightarrow 0, 0, 1, 1, g\rangle$	JC	Sec. IV A
		1 resonator, 3 qubits	$\omega_a + \omega_{q1} = \omega_{q2} + \omega_{q3}$	$ 1, e, g, g\rangle \rightarrow 0, g, e, e\rangle$	JC	Sec. IV A
		3 resonators, 1 qubit	$\omega_a + \omega_b + \omega_c = \omega_q$	$ 1, 1, 1, g\rangle \rightarrow 0, 0, 0, e\rangle$	Rabi	Sec. IV A
		4 resonators, 1 qubit	$\omega_a + \omega_b + \omega_c = \omega_d$	$ 1, 1, 1, 0, g\rangle \rightarrow 0, 0, 0, 1, g\rangle$	JC	Sec. IV A
		2 resonators, 2 qubits	$\omega_a = \omega_b + \omega_{q1} + \omega_{q2}$	$ 0, 1, e, e\rangle \rightarrow 1, 0, g, g\rangle$	Rabi	Sec. IV A
		1 resonator, 3 qubits	$\omega_a = \omega_{q1} + \omega_{q2} + \omega_{q3}$	$ 0, e, e, e\rangle \rightarrow 1, g, g, g\rangle$	Rabi	Sec. IV A
		3 resonators, 1 qubit	$\omega_a + \omega_b + \omega_c = \omega_q$	$ 0, 0, 0, e\rangle \rightarrow 1, 1, 1, g\rangle$	Rabi	Sec. IV A
Non-degenerate four-wave mixing	Type II (3 inputs, 1 output)	4 resonators, 1 qubit	$\omega_a = \omega_b + \omega_c + \omega_d$	$ 1, 0, 0, g\rangle \rightarrow 0, 1, 1, g\rangle$	Rabi	Sec. IV A
		2 resonators, 2 qubits	$\omega_a = \omega_b + \omega_{q1} + \omega_{q2}$	$ 0, 1, e, e\rangle \rightarrow 1, 0, g, g\rangle$	Rabi	Sec. IV A
		1 resonator, 3 qubits	$\omega_a = \omega_{q1} + \omega_{q2} + \omega_{q3}$	$ 0, e, e, e\rangle \rightarrow 1, g, g, g\rangle$	Rabi	Sec. IV A
	Type III (1 input, 3 outputs)	3 resonators, 1 qubit	$\omega_a + \omega_b + \omega_c = \omega_q$	$ 0, 0, 0, e\rangle \rightarrow 1, 1, 1, g\rangle$	Rabi	Sec. IV A
		4 resonators, 1 qubit	$\omega_a = \omega_b + \omega_c + \omega_d$	$ 1, 0, 0, 0, g\rangle \rightarrow 0, 1, 1, 1, g\rangle$	Rabi	Sec. IV A

processes described here to create various superposition states with applications in quantum information processing, and we expect that adding the capabilities of nonlinear optics at the single-photon level to current quantum technology will spawn many more important applications. Considering an experimental implementation, we have shown that most, if not all, of the processes discussed here can be realized with currently available technology in circuit QED. Given that ultrastrong light-matter coupling has been demonstrated in several other solid-state systems as well, the processes proposed here could potentially also be implemented in other setups in the future.

ACKNOWLEDGMENTS

A.F.K. acknowledges support from a JSPS Postdoctoral Fellowship for Overseas Researchers. A.M. and F.N. acknowledge the support of a grant from the John Templeton Foundation. F.N. was also partially supported by the RIKEN iTHES Project, the MURI Center for Dynamic Magneto-Optics via AFOSR Award No. FA9550-14-1-0040, the Japan Society for the Promotion of Science (KAKENHI), the IMPACT program of JST, JSPS-RFBR Grant No. 17-52-50023, and CREST Grant No. JPMJCR1676.

APPENDIX A: CLASSICAL DESCRIPTION OF NONLINEAR OPTICAL PHENOMENA

Here we give a few examples showing how mixing of classical waves can be explained classically by applying the principal relation of nonlinear optics,

$$\begin{aligned} \mathbf{P} &= \epsilon_0(\chi^{(1)}\mathbf{E} + \chi^{(2)}\mathbf{E}^2 + \chi^{(3)}\mathbf{E}^3 + \dots) \\ &= \mathbf{P}^{(1)} + \mathbf{P}^{(2)} + \mathbf{P}^{(3)} + \dots \end{aligned} \quad (\text{A1})$$

In this pedagogical introduction to nonlinear optics, based on Ref. [1], we give the classical explanations of a few standard wave-mixing processes by applying the lowest-order required nonlinear polarization $\mathbf{P}^{(n)}$ and the corresponding nonlinear susceptibility $\chi^{(n)}$. Our examples include the linear (Pockels) and quadratic (Kerr) electro-optical phenomena. Second-harmonic generation in a $\chi^{(2)}$ medium was already treated in Sec. II A.

1. Wave mixing in a $\chi^{(2)}$ medium and the Pockels effect

Assume that two monochromatic scalar electric waves, $E_1(t) = E_{10} \cos(\omega_1 t)$ and $E_2(t) = E_{20} \cos(\omega_2 t)$, are applied to a medium described by the second-order frequency-independent susceptibility $\chi^{(2)}$. Then, the induced second-order polarization $P^{(2)}$ is given by

$$\begin{aligned} P^{(2)} &= \epsilon_0 \chi^{(2)} E^2 = \epsilon_0 \chi^{(2)} \{E_{10} \cos(\omega_1 t) + E_{20} \cos(\omega_2 t)\}^2 \\ &= \epsilon_0 \chi^{(2)} \{E_{10}^2 \cos^2(\omega_1 t) + E_{20}^2 \cos^2(\omega_2 t) \\ &\quad + 2E_{10} E_{20} \cos(\omega_1 t) \cos(\omega_2 t)\} \\ &= \frac{1}{2} \epsilon_0 \chi^{(2)} \{E_{10}^2 [1 + \cos(2\omega_1 t)] + E_{20}^2 [1 + \cos(2\omega_2 t)] \\ &\quad + 2E_{10} E_{20} (\cos[(\omega_1 - \omega_2)t] + \cos[(\omega_1 + \omega_2)t])\} \end{aligned}$$

$$\begin{aligned} &= \frac{1}{2} \epsilon_0 \chi^{(2)} \{(E_{10}^2 + E_{20}^2) + E_{10}^2 \cos(2\omega_1 t) \\ &\quad + E_{20}^2 \cos(2\omega_2 t) + 2E_{10} E_{20} \cos[(\omega_1 - \omega_2)t] \\ &\quad + 2E_{10} E_{20} \cos[(\omega_1 + \omega_2)t]\} \\ &\equiv P_0^{(2)} + P_{2\omega_1}^{(2)} + P_{2\omega_2}^{(2)} + P_{\omega_1 - \omega_2}^{(2)} + P_{\omega_1 + \omega_2}^{(2)}, \end{aligned} \quad (\text{A2})$$

where the induced second-order nonlinear polarization $P_{\omega_x}^{(2)}$, oscillating with frequency $\omega_x = 0, 2\omega_1, \dots$, is defined by the corresponding ω_x -dependent term in the second-last equation in Eq. (A2).

We see that this process can be interpreted as mixing of two waves with frequencies ω_1 and ω_2 . Alternatively, in a general case, this effect can be interpreted as six-wave mixing if we include also the four output (mixed) frequencies $2\omega_1$, $2\omega_2$, $|\omega_1 - \omega_2|$, and $\omega_1 + \omega_2$. In a quantum description, the latter interpretation is conventionally applied.

In a special case, let us assume that $\omega_2 = 0$; then $E_2 = E_{20} = \text{constant}$, and

$$P_{\omega_1 - \omega_2}^{(2)} + P_{\omega_1 + \omega_2}^{(2)} = 2P_{\omega_1}^{(2)} = \epsilon_0(2\chi^{(2)}E_{20})E_1(t). \quad (\text{A3})$$

We see that the effective first-order-like susceptibility $\chi_{\text{eff}}^{(1)} \equiv 2\chi^{(2)}E_{20}$ is proportional to the amplitude of the constant electric field. This phenomenon is usually referred to as the (linear) Pockels effect or linear electro-optical effect.

A few comments can be made on the momentum (and energy) conservation when fields of frequencies ω_1 and ω_2 are mixed to generate fields with sum ($\omega_+ = \omega_1 + \omega_2$) and difference ($\omega_- = |\omega_1 - \omega_2|$) frequencies. These new fields can be amplified depending on which momentum condition $\mathbf{k}_+ = \mathbf{k}_1 + \mathbf{k}_2$ or $\mathbf{k}_- = \mathbf{k}_1 - \mathbf{k}_2$ is satisfied for the corresponding wave vectors \mathbf{k}_j . Usually only one of these conditions is satisfied. If both conditions are fulfilled, then the wave mixing has a local character. For example, if $\omega_1 = \omega_2 \equiv \omega$ and $\mathbf{k}_1 = \mathbf{k}_2 \equiv \mathbf{k}$, then $\omega_+ = 2\omega$, $\omega_- = 0$, $k_+ = 2k$, and $k_- = 0$.

2. Third-harmonic generation in a $\chi^{(3)}$ medium

Assume that a monochromatic electric wave $E(t) = E_0 \cos(\omega t)$ is applied to a medium described solely by a third-order susceptibility $\chi^{(3)}$. Then we observe

$$\begin{aligned} P^{(3)} &= \epsilon_0 \chi^{(3)} E^3 = \epsilon_0 \chi^{(3)} E_0^3 \cos^3(\omega t) \\ &= \epsilon_0 \chi^{(3)} E_0^3 \left[\frac{3 \cos(\omega t) + \cos(3\omega t)}{4} \right] \\ &= \frac{3}{4} \epsilon_0 \chi^{(3)} E_0^3 \cos(\omega t) + \frac{1}{4} \epsilon_0 \chi^{(3)} E_0^3 \cos(3\omega t) \\ &= P_\omega^{(3)} + P_{3\omega}^{(3)}, \end{aligned} \quad (\text{A4})$$

where the term $P_{3\omega}^{(3)}$ describes the induced polarization, oscillating with triple the frequency of the input field, which can be interpreted as third-harmonic generation.

3. Wave mixing in a $\chi^{(3)}$ medium and the Kerr effect

Assume that two monochromatic electric beams, $E_1(t) = E_{10} \cos(\omega_1 t)$ and $E_2(t) = E_{20} \cos(\omega_2 t)$, are applied to a medium described by a third-order susceptibility $\chi^{(3)}$, and that $\chi^{(3)}$ is frequency independent. Then the third-order induced

polarization $P^{(3)}$ of the medium is given by

$$\begin{aligned} P^{(3)} &= \epsilon_0 \chi^{(3)} E^3 = \epsilon_0 \chi^{(3)} [E_{10} \cos(\omega_1 t) + E_{20} \cos(\omega_2 t)]^3 \\ &= P_{\omega_1}^{(3)} + P_{\omega_2}^{(3)} + P_{3\omega_1}^{(3)} + P_{3\omega_2}^{(3)} + P_{2\omega_1 - \omega_2}^{(3)} \\ &\quad + P_{2\omega_1 + \omega_2}^{(3)} + P_{2\omega_2 - \omega_1}^{(3)} + P_{2\omega_2 + \omega_1}^{(3)}, \end{aligned} \quad (\text{A5})$$

where we do not give (except two terms) an explicit form of these induced third-order nonlinear polarizations $P_{\omega_x}^{(3)}$, but only indicate their frequencies ω_x .

Analogously to wave mixing in a $\chi^{(2)}$ medium, one can interpret this process as mixing of two waves with frequencies ω_1 and ω_2 . Alternatively, this effect, in a general case, can be interpreted as mixing of eight waves (including the output waves) with frequencies ω_1 , ω_2 , $3\omega_1$, $3\omega_2$, $|2\omega_1 \pm \omega_2|$, and $|2\omega_2 \pm \omega_1|$. In a quantum description, the latter convention is usually applied.

In a special case, we have

$$P_{2\omega_2 \pm \omega_1}^{(3)} = \frac{3}{4} \epsilon_0 \chi^{(3)} E_{20}^2 E_{10} \cos[(2\omega_2 \pm \omega_1)t]. \quad (\text{A6})$$

If we assume that $\omega_2 = 0$, we obtain

$$P_{2\omega_2 \pm \omega_1}^{(3)} = \frac{3}{4} \epsilon_0 \chi^{(3)} E_{20}^2 E_{10} \cos(\omega_1 t) \equiv \epsilon_0 \chi_{\text{eff}}^{(1)} E_1(t). \quad (\text{A7})$$

Thus, the effective first-order-like susceptibility $\chi_{\text{eff}}^{(1)} \equiv \frac{3}{4} \chi^{(3)} E_{20}^2$ is proportional to the square of the constant electric field $E_2(t) = E_{20}$. This is a standard classical explanation of the Kerr effect, which is also referred to as the quadratic electro-optical effect.

APPENDIX B: PERTURBATION THEORY

In this Appendix, we show how to derive the expression for the effective coupling given in Eq. (10). In all processes we considered in Secs. III and IV, there is an initial state $|i\rangle$ and a final state $|f\rangle$ connected by the effective coupling in an effective interaction Hamiltonian

$$\hat{H}_{\text{int}}^{\text{eff}} = g_{\text{eff}} |f\rangle \langle i| + \text{H.c.} \quad (\text{B1})$$

As stated in Sec. II B, if the shortest path between $|i\rangle$ and $|f\rangle$ is an n th-order process, the effective coupling g_{eff} is given to lowest order by

$$g_{\text{eff}} = \sum_{j_1, j_2, \dots, j_{n-1}} \frac{V_{fj_{n-1}} \dots V_{j_2 j_1} V_{j_1 i}}{(E_i - E_{j_1})(E_i - E_{j_2}) \dots (E_i - E_{j_{n-1}})}, \quad (\text{B2})$$

where the sum goes over all virtual transitions forming n -step paths between $|i\rangle$ and $|f\rangle$. The formula in Eq. (B2) can be derived by considering the Dyson series of the time evolution operator in the interaction picture,

$$\begin{aligned} \hat{U}_I(t, t_0) &= 1 - i \int_{t_0}^t dt' \hat{H}_{\text{int}}(t') \\ &\quad + (-i)^2 \int_{t_0}^t dt' \int_{t_0}^{t'} dt'' \hat{H}_{\text{int}}(t') \hat{H}_{\text{int}}(t'') + \dots, \end{aligned} \quad (\text{B3})$$

when the interaction Hamiltonian \hat{H}_{int} is time-independent. Assuming the system starts in the eigenstate $|i\rangle$ of the noninteracting Hamiltonian at time t_0 , the probability of

the transition $|i\rangle \rightarrow |f\rangle$ is given to lowest (n th) order by the n th-order term in Eq. (B3), $U_I^{(n)}(t, t_0)$, through

$$\begin{aligned} P(|i\rangle \rightarrow |f\rangle) &= |\langle f | \hat{U}_I^{(n)}(t, t_0) | i \rangle|^2 = \frac{(1 - e^{i(E_f - E_i)})^2}{(E_f - E_i)^2} \\ &\quad \times \left| \sum_{j_1, j_2, \dots, j_{n-1}} \frac{V_{fj_{n-1}} \dots V_{j_2 j_1} V_{j_1 i}}{(E_i - E_{j_1})(E_i - E_{j_2}) \dots (E_i - E_{j_{n-1}})} \right|^2, \end{aligned} \quad (\text{B4})$$

which in the limit $t \rightarrow \infty$ gives the transition rate

$$\begin{aligned} W_{(|i\rangle \rightarrow |f\rangle)} &= 2\pi \delta(E_f - E_i) \\ &\quad \times \left| \sum_{j_1, j_2, \dots, j_{n-1}} \frac{V_{fj_{n-1}} \dots V_{j_2 j_1} V_{j_1 i}}{(E_i - E_{j_1})(E_i - E_{j_2}) \dots (E_i - E_{j_{n-1}})} \right|^2. \end{aligned} \quad (\text{B5})$$

This is just Fermi's golden rule, showing that the effective Hamiltonian in Eq. (B1) with the coupling strength g_{eff} given by Eq. (10) gives the correct coupling matrix element between $|i\rangle$ and $|f\rangle$.

APPENDIX C: FOUR-WAVE MIXING WITH TWO DEGENERATE FREQUENCIES

For completeness, we here show, in Fig. 10, schematic representations of the four degenerate four-wave-mixing processes where two frequencies are degenerate (omitted from Fig. 5). Analogs for these processes can be constructed in the same way as for the other four-wave mixing processes treated in Sec. IV and listed in Table III. The most obvious setup is three resonators all coupled to a single qubit. In that case, the process $|2, 0, 0, g\rangle \leftrightarrow |0, 1, 1, g\rangle$ corresponds to the type-I mixing shown in the figure. Similarly, $|2, 1, 0, g\rangle \leftrightarrow |0, 0, 1, e\rangle$ realizes analogs of the pictured type-II (\rightarrow) and type-III (\leftarrow) processes, respectively.

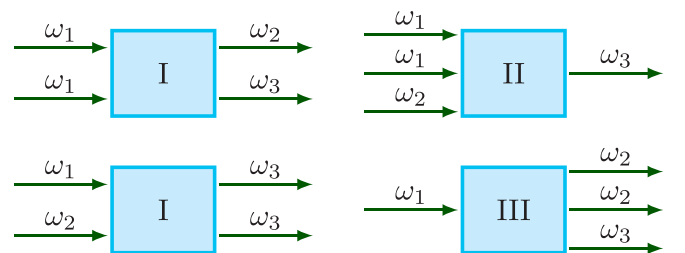


FIG. 10. Schematic representations (Feynman-like diagrams) of the four-wave-mixing processes with two degenerate frequencies. Going clockwise from the upper left corner, they are as follows: type-I four-wave mixing with the frequencies of the two incoming signals degenerate ($2\omega_1 = \omega_2 + \omega_3$), type-II four-wave mixing with the frequencies of two of the incoming signals degenerate ($2\omega_1 + \omega_2 = \omega_3$), type-III four-wave mixing with the frequencies of two of the outgoing signals degenerate ($\omega_1 = 2\omega_2 + \omega_3$), and type-I four-wave mixing with the frequencies of the two outgoing signals degenerate ($\omega_1 + \omega_2 = 2\omega_3$).

Just as for the nondegenerate mixing processes discussed in Secs. III A 2 and IV A 2, additional setups become possible if we allow at least one of the excitations to be hosted in a qubit. With two resonators coupled to a single qubit, the two type-I mixing processes shown in Fig. 10 could be emulated by $|2,0,g\rangle \leftrightarrow |0,1,e\rangle$, which we recognize as the analog of type-I hyper-Raman scattering already treated in

Sec. IV C 2. The pictured type-II and type-III mixing could similarly be emulated by, e.g., the process $|2,1,g\rangle \leftrightarrow |0,0,e\rangle$. In the same way, a setup with a single resonator coupled to two qubits could realize analogs of the pictured type-I processes through the transition $|2,g,g\rangle \leftrightarrow |0,e,e\rangle$, and of the pictured type-II and type-III processes through the transition $|2,e,g\rangle \leftrightarrow |0,g,e\rangle$.

-
- [1] P. A. Lindsay, *Introduction to Quantum Electronics* (Pitman, London, 1975).
 - [2] S. Kielich, *Molecular Nonlinear Optics* (Nauka, Moscow, 1981).
 - [3] Y. R. Shen, *The Principles of Nonlinear Optics* (Wiley, New York, 1984).
 - [4] R. W. Boyd, *Nonlinear Optics*, 3rd ed. (Elsevier, Amsterdam, 2008).
 - [5] P. A. Franken, A. E. Hill, C. W. Peters, and G. Weinreich, Generation of Optical Harmonics, *Phys. Rev. Lett.* **7**, 118 (1961).
 - [6] F. V. Bunkin, Y. A. Kravtsov, and G. A. Lyakhov, Acoustic analogues of nonlinear-optics phenomena, *Sov. Phys. Usp.* **29**, 607 (1986).
 - [7] M. F. Hamilton and D. T. Blackstock (eds.), *Nonlinear Acoustics: Theory and Applications* (Academic Press, New York, 1998).
 - [8] M. G. Cottam (ed.), *Linear and Nonlinear Spin Waves in Magnetic Films and Superlattices* (World Scientific, Singapore, 1994).
 - [9] G. Lenz, P. Meystre, and E. M. Wright, Nonlinear Atom Optics, *Phys. Rev. Lett.* **71**, 3271 (1993).
 - [10] S. L. Rolston and W. D. Phillips, Nonlinear and quantum atom optics, *Nature (London)* **416**, 219 (2002).
 - [11] S. Savel'ev, A. L. Rakhmanov, V. A. Yampol'skii, and F. Nori, Analogues of nonlinear optics using terahertz Josephson plasma waves in layered superconductors, *Nat. Phys.* **2**, 521 (2006).
 - [12] M. Kauranen and A. V. Zayats, Nonlinear plasmonics, *Nat. Photonics* **6**, 737 (2012).
 - [13] I. Buluta and F. Nori, Quantum simulators, *Science* **326**, 108 (2009).
 - [14] P. D. Nation, J. R. Johansson, M. P. Blencowe, and F. Nori, Colloquium: Stimulating uncertainty: Amplifying the quantum vacuum with superconducting circuits, *Rev. Mod. Phys.* **84**, 1 (2012).
 - [15] I. M. Georgescu, S. Ashhab, and F. Nori, Quantum simulation, *Rev. Mod. Phys.* **86**, 153 (2014).
 - [16] J. Q. You and F. Nori, Atomic physics and quantum optics using superconducting circuits, *Nature (London)* **474**, 589 (2011).
 - [17] I. I. Rabi, Space quantization in a gyrating magnetic field, *Phys. Rev.* **51**, 652 (1937).
 - [18] G. Günter, A. A. Anappara, J. Hees, A. Sell, G. Biasiol, L. Sorba, S. De Liberato, C. Ciuti, A. Tredicucci, A. Leitenstorfer, and R. Huber, Sub-cycle switch-on of ultrastrong light-matter interaction, *Nature (London)* **458**, 178 (2009).
 - [19] P. Forn-Díaz, J. Lisenfeld, D. Marcos, J. J. García-Ripoll, E. Solano, C. J. P. M. Harmans, and J. E. Mooij, Observation of the Bloch-Siegert Shift in a Qubit-Oscillator System in the Ultrastrong Coupling Regime, *Phys. Rev. Lett.* **105**, 237001 (2010).
 - [20] T. Niemczyk, F. Deppe, H. Huebl, E. P. Menzel, F. Hocke, M. J. Schwarz, J. J. García-Ripoll, D. Zueco, T. Hücker, E. Solano, A. Marx, and R. Gross, Circuit quantum electrodynamics in the ultrastrong-coupling regime, *Nat. Phys.* **6**, 772 (2010).
 - [21] Y. Todorov, A. M. Andrews, R. Colombelli, S. De Liberato, C. Ciuti, P. Klang, G. Strasser, and C. Sirtori, Ultrastrong Light-Matter Coupling Regime with Polariton Dots, *Phys. Rev. Lett.* **105**, 196402 (2010).
 - [22] T. Schwartz, J. A. Hutchison, C. Genet, and T. W. Ebbesen, Reversible Switching of Ultrastrong Light-Molecule Coupling, *Phys. Rev. Lett.* **106**, 196405 (2011).
 - [23] G. Scalari, C. Maissen, D. Turcinkova, D. Hagenmuller, S. De Liberato, C. Ciuti, C. Reichl, D. Schuh, W. Wegscheider, M. Beck, and J. Faist, Ultrastrong coupling of the cyclotron transition of a 2D electron gas to a THz metamaterial, *Science* **335**, 1323 (2012).
 - [24] M. Geiser, F. Castellano, G. Scalari, M. Beck, L. Nevou, and J. Faist, Ultrastrong Coupling Regime and Plasmon Polaritons in Parabolic Semiconductor Quantum Wells, *Phys. Rev. Lett.* **108**, 106402 (2012).
 - [25] S. Kéna-Cohen, S. A. Maier, and D. D. C. Bradley, Ultrastrongly coupled exciton-polaritons in metal-clad organic semiconductor microcavities, *Adv. Opt. Mater.* **1**, 827 (2013).
 - [26] S. Gambino, M. Mazzeo, A. Genco, O. Di Stefano, S. Savasta, S. Patanè, D. Ballarini, F. Mangione, G. Lerario, D. Sanvitto, and G. Gigli, Exploring light-matter interaction phenomena under ultrastrong coupling regime, *ACS Photonics* **1**, 1042 (2014).
 - [27] C. Maissen, G. Scalari, F. Valmorra, M. Beck, J. Faist, S. Cibella, R. Leoni, C. Reichl, C. Charpentier, and W. Wegscheider, Ultrastrong coupling in the near field of complementary splitting resonators, *Phys. Rev. B* **90**, 205309 (2014).
 - [28] M. Goryachev, W. G. Farr, D. L. Creedon, Y. Fan, M. Kostylev, and M. E. Tobar, High-Cooperativity Cavity QED with Magnons at Microwave Frequencies, *Phys. Rev. Appl.* **2**, 054002 (2014).
 - [29] A. Baust, E. Hoffmann, M. Haeberlein, M. J. Schwarz, P. Eder, J. Goetz, F. Wulschner, E. Xie, L. Zhong, F. Quijandría, D. Zueco, J.-J. García Ripoll, L. García-Álvarez, G. Romero, E. Solano, K. G. Fedorov, E. P. Menzel, F. Deppe, A. Marx, and R. Gross, Ultrastrong coupling in two-resonator circuit QED, *Phys. Rev. B* **93**, 214501 (2016).
 - [30] P. Forn-Díaz, J. J. García-Ripoll, B. Peropadre, J.-L. Orgiazzi, M. A. Yurtalan, R. Belyansky, C. M. Wilson, and A. Lupascu, Ultrastrong coupling of a single artificial atom to an electromagnetic continuum in the nonperturbative regime, *Nat. Phys.* **13**, 39 (2017).
 - [31] F. Yoshihara, T. Fuse, S. Ashhab, K. Kakuyanagi, S. Saito, and K. Semba, Superconducting qubit-oscillator circuit beyond the ultrastrong-coupling regime, *Nat. Phys.* **13**, 44 (2017).

- [32] Z. Chen, Y. Wang, T. Li, L. Tian, Y. Qiu, K. Inomata, F. Yoshihara, S. Han, F. Nori, J. S. Tsai, and J. Q. You, Multiphoton sideband transitions in an ultrastrongly coupled circuit quantum electrodynamics system, [arXiv:1602.01584](#).
- [33] J. George, T. Chervy, A. Shalabney, E. Devaux, H. Hiura, C. Genet, and T. W. Ebbesen, Multiple Rabi Splittings under Ultrastrong Vibrational Coupling, *Phys. Rev. Lett.* **117**, 153601 (2016).
- [34] N. K. Langford, R. Sagastizabal, M. Kounalakis, C. Dickel, A. Bruno, F. Luthi, D. J. Thoen, A. Endo, and L. DiCarlo, Experimentally simulating the dynamics of quantum light and matter at ultrastrong coupling, [arXiv:1610.10065](#).
- [35] J. Braumüller, M. Marthaler, A. Schneider, A. Stehli, H. Rotzinger, M. Weides, and A. V. Ustinov, Analog quantum simulation of the Rabi model in the ultrastrong-coupling regime, [arXiv:1611.08404](#).
- [36] F. Yoshihara, T. Fuse, S. Ashhab, K. Kakuyanagi, S. Saito, and K. Semba, Characteristic spectra of circuit quantum electrodynamics systems from the ultrastrong to the deep strong coupling regime, *Phys. Rev. A* **95**, 053824 (2017).
- [37] A. Wallraff, D. I. Schuster, A. Blais, L. Frunzio, R.-S. Huang, J. Majer, S. Kumar, S. M. Girvin, and R. J. Schoelkopf, Strong coupling of a single photon to a superconducting qubit using circuit quantum electrodynamics, *Nature (London)* **431**, 162 (2004).
- [38] A. Blais, R.-S. Huang, A. Wallraff, S. M. Girvin, and R. J. Schoelkopf, Cavity quantum electrodynamics for superconducting electrical circuits: An architecture for quantum computation, *Phys. Rev. A* **69**, 062320 (2004).
- [39] Z.-L. Xiang, S. Ashhab, J. Q. You, and F. Nori, Hybrid quantum circuits: Superconducting circuits interacting with other quantum systems, *Rev. Mod. Phys.* **85**, 623 (2013).
- [40] S. De Liberato, C. Ciuti, and I. Carusotto, Quantum Vacuum Radiation Spectra from a Semiconductor Microcavity with a Time-Modulated Vacuum Rabi Frequency, *Phys. Rev. Lett.* **98**, 103602 (2007).
- [41] S. Ashhab and F. Nori, Qubit-oscillator systems in the ultrastrong-coupling regime and their potential for preparing nonclassical states, *Phys. Rev. A* **81**, 042311 (2010).
- [42] X. Cao, J. Q. You, H. Zheng, A. G. Kofman, and F. Nori, Dynamics and quantum Zeno effect for a qubit in either a low- or high-frequency bath beyond the rotating-wave approximation, *Phys. Rev. A* **82**, 022119 (2010).
- [43] J. Casanova, G. Romero, I. Lizuain, J. J. García-Ripoll, and E. Solano, Deep Strong Coupling Regime of the Jaynes-Cummings Model, *Phys. Rev. Lett.* **105**, 263603 (2010).
- [44] F. Beaudoin, J. M. Gambetta, and A. Blais, Dissipation and ultrastrong coupling in circuit QED, *Phys. Rev. A* **84**, 043832 (2011).
- [45] A. Ridolfo, M. Leib, S. Savasta, and M. J. Hartmann, Photon Blockade in the Ultrastrong Coupling Regime, *Phys. Rev. Lett.* **109**, 193602 (2012).
- [46] R. Stassi, A. Ridolfo, O. Di Stefano, M. J. Hartmann, and S. Savasta, Spontaneous Conversion from Virtual to Real Photons in the Ultrastrong-Coupling Regime, *Phys. Rev. Lett.* **110**, 243601 (2013).
- [47] S. De Liberato, Light-Matter Decoupling in the Deep Strong Coupling Regime: The Breakdown of the Purcell Effect, *Phys. Rev. Lett.* **112**, 016401 (2014).
- [48] E. Sanchez-Burillo, D. Zueco, J. J. Garcia-Ripoll, and L. Martin-Moreno, Scattering in the Ultrastrong Regime: Nonlinear Optics with One Photon, *Phys. Rev. Lett.* **113**, 263604 (2014).
- [49] J. Lolli, A. Baksic, D. Nagy, V. E. Manucharyan, and C. Ciuti, Ancillary Qubit Spectroscopy of Vacua in Cavity and Circuit Quantum Electrodynamics, *Phys. Rev. Lett.* **114**, 183601 (2015).
- [50] M. Cirio, S. De Liberato, N. Lambert, and F. Nori, Ground State Electroluminescence, *Phys. Rev. Lett.* **116**, 113601 (2016).
- [51] O. Di Stefano, R. Stassi, L. Garziano, A. F. Kockum, S. Savasta, and F. Nori, Feynman-diagrams approach to the quantum Rabi model for ultrastrong cavity QED: Stimulated emission and reabsorption of virtual particles dressing a physical excitation, *New J. Phys.* **19**, 053010 (2017).
- [52] K. K. W. Ma and C. K. Law, Three-photon resonance and adiabatic passage in the large-detuning Rabi model, *Phys. Rev. A* **92**, 023842 (2015).
- [53] L. Garziano, R. Stassi, V. Macrì, A. F. Kockum, S. Savasta, and F. Nori, Multiphoton quantum Rabi oscillations in ultrastrong cavity QED, *Phys. Rev. A* **92**, 063830 (2015).
- [54] L. Garziano, V. Macrì, R. Stassi, O. Di Stefano, F. Nori, and S. Savasta, One Photon Can Simultaneously Excite Two or More Atoms, *Phys. Rev. Lett.* **117**, 043601 (2016).
- [55] A. F. Kockum, V. Macrì, L. Garziano, S. Savasta, and F. Nori, Frequency conversion in ultrastrong cavity QED, [arXiv:1701.07973](#) [Sci. Rep. (to be published)].
- [56] R. Stassi, V. Macrì, A. F. Kockum, O. Di Stefano, A. Miranowicz, S. Savasta, and F. Nori, Quantum nonlinear optics without photons, [arXiv:1702.00660](#).
- [57] M. H. Devoret and R. J. Schoelkopf, Superconducting circuits for quantum information: An outlook, *Science* **339**, 1169 (2013).
- [58] D. E. Chang, V. Vuletić, and M. D. Lukin, Quantum nonlinear optics—photon by photon, *Nat. Photonics* **8**, 685 (2014).
- [59] B. Peropadre, G. G. Guerreschi, J. Huh, and A. Aspuru-Guzik, Proposal for Microwave Boson Sampling, *Phys. Rev. Lett.* **117**, 140505 (2016).
- [60] E. T. Jaynes and F. W. Cummings, Comparison of quantum and semiclassical radiation theories with application to the beam maser, *Proc. IEEE* **51**, 89 (1963).
- [61] T. P. Orlando, J. E. Mooij, L. Tian, C. H. van der Wal, L. S. Levitov, S. Lloyd, and J. J. Mazo, Superconducting persistent-current qubit, *Phys. Rev. B* **60**, 15398 (1999).
- [62] T. Lindström, C. H. Webster, J. E. Healey, M. S. Colclough, C. M. Muirhead, and A. Y. Tzalenchuk, Circuit QED with a flux qubit strongly coupled to a coplanar transmission line resonator, *Supercond. Sci. Technol.* **20**, 814 (2007).
- [63] F. Deppe, M. Mariantoni, E. P. Menzel, A. Marx, S. Saito, K. Kakuyanagi, H. Tanaka, T. Meno, K. Semba, H. Takayanagi, E. Solano, and R. Gross, Two-photon probe of the Jaynes-Cummings model and controlled symmetry breaking in circuit QED, *Nat. Phys.* **4**, 686 (2008).
- [64] J. Bourassa, J. M. Gambetta, A. A. Abdumalikov, O. Astafiev, Y. Nakamura, and A. Blais, Ultrastrong coupling regime of cavity QED with phase-biased flux qubits, *Phys. Rev. A* **80**, 032109 (2009).
- [65] K. Moon and S. M. Girvin, Theory of Microwave Parametric Down-Conversion and Squeezing Using Circuit QED, *Phys. Rev. Lett.* **95**, 140504 (2005).
- [66] J. R. Johansson, P. D. Nation, and F. Nori, QuTiP: An open-source Python framework for the dynamics of open quantum systems, *Comput. Phys. Commun.* **183**, 1760 (2012).

- [67] J. R. Johansson, P. D. Nation, and F. Nori, QuTiP 2: A Python framework for the dynamics of open quantum systems, *Comput. Phys. Commun.* **184**, 1234 (2013).
- [68] A. Miranowicz and S. Kielich, Quantum-statistical theory of Raman scattering processes, *Adv. Chem. Phys.* **85**(III), 531 (1994).
- [69] M. Göppert-Mayer, Über elementarakte mit zwei quantensprün-gen, *Ann. Phys.* **401**, 273 (1931).
- [70] M. Boissonneault, J. M. Gambetta, and A. Blais, Dispersive regime of circuit QED: Photon-dependent qubit dephasing and relaxation rates, *Phys. Rev. A* **79**, 013819 (2009).
- [71] S. E. Nigg, H. Paik, B. Vlastakis, G. Kirchmair, S. Shankar, L. Frunzio, M. H. Devoret, R. J. Schoelkopf, and S. M. Girvin, Black-Box Superconducting Circuit Quantization, *Phys. Rev. Lett.* **108**, 240502 (2012).
- [72] G. Zhu, D. G. Ferguson, V. E. Manucharyan, and J. Koch, Circuit QED with fluxonium qubits: Theory of the dispersive regime, *Phys. Rev. B* **87**, 024510 (2013).
- [73] G. Kirchmair, B. Vlastakis, Z. Leghtas, S. E. Nigg, H. Paik, E. Ginossar, M. Mirrahimi, L. Frunzio, S. M. Girvin, and R. J. Schoelkopf, Observation of quantum state collapse and revival due to the single-photon Kerr effect, *Nature (London)* **495**, 205 (2013).
- [74] E. T. Holland, B. Vlastakis, R. W. Heeres, M. J. Reagor, U. Vool, Z. Leghtas, L. Frunzio, G. Kirchmair, M. H. Devoret, M. Mirrahimi, and R. J. Schoelkopf, Single-Photon-Resolved Cross-Kerr Interaction for Autonomous Stabilization of Photon-Number States, *Phys. Rev. Lett.* **115**, 180501 (2015).
- [75] B. Fan, A. F. Kockum, J. Combes, G. Johansson, I.-C. Hoi, C. M. Wilson, P. Delsing, G. J. Milburn, and T. M. Stace, Breakdown of the Cross-Kerr Scheme for Photon Counting, *Phys. Rev. Lett.* **110**, 053601 (2013).
- [76] I.-C. Hoi, A. F. Kockum, T. Palomaki, T. M. Stace, B. Fan, L. Tornberg, S. R. Sathyamoorthy, G. Johansson, P. Delsing, and C. M. Wilson, Giant Cross-Kerr Effect for Propagating Microwaves Induced by an Artificial Atom, *Phys. Rev. Lett.* **111**, 053601 (2013).
- [77] M. Stern, G. Catelani, Y. Kubo, C. Grezes, A. Bienfait, D. Vion, D. Esteve, and P. Bertet, Flux Qubits with Long Coherence Times for Hybrid Quantum Circuits, *Phys. Rev. Lett.* **113**, 123601 (2014).
- [78] J.-L. Orgiazzi, C. Deng, D. Layden, R. Marchildon, F. Kitapli, F. Shen, M. Bal, F. R. Ong, and A. Lupascu, Flux qubits in a planar circuit quantum electrodynamics architecture: Quantum control and decoherence, *Phys. Rev. B* **93**, 104518 (2016).
- [79] J. Q. You, X. Hu, S. Ashhab, and F. Nori, Low-decoherence flux qubit, *Phys. Rev. B* **75**, 140515 (2007).
- [80] F. Yan, S. Gustavsson, A. Kamal, J. Birenbaum, A. P. Sears, D. Hover, T. J. Gudmundsen, D. Rosenberg, G. Samach, S. Weber, J. L. Yoder, T. P. Orlando, J. Clarke, A. J. Kerman, and W. D. Oliver, The flux qubit revisited to enhance coherence and reproducibility, *Nat. Commun.* **7**, 12964 (2016).
- [81] C. Rigetti, J. M. Gambetta, S. Poletto, B. L. T. Plourde, J. M. Chow, A. D. Córcoles, J. A. Smolin, S. T. Merkel, J. R. Rozen, G. A. Keefe, M. B. Rothwell, M. B. Ketchen, and M. Steffen, Superconducting qubit in a waveguide cavity with a coherence time approaching 0.1 ms, *Phys. Rev. B* **86**, 100506 (2012).
- [82] X. Y. Jin, A. Kamal, A. P. Sears, T. Gudmundsen, D. Hover, J. Miloshi, R. Slattery, F. Yan, J. Yoder, T. P. Orlando, S. Gustavsson, and W. D. Oliver, Thermal and Residual Excited-State Population in a 3D Transmon Qubit, *Phys. Rev. Lett.* **114**, 240501 (2015).
- [83] A. Megrant, C. Neill, R. Barends, B. Chiaro, Y. Chen, L. Feigl, J. Kelly, E. Lucero, M. Mariantoni, P. J. J. O’Malley, D. Sank, A. Vainsencher, J. Wenner, T. C. White, Y. Yin, J. Zhao, C. J. Palmstrøm, J. M. Martinis, and A. N. Cleland, Planar superconducting resonators with internal quality factors above one million, *Appl. Phys. Lett.* **100**, 113510 (2012).
- [84] M. Reagor, H. Paik, G. Catelani, L. Sun, C. Axline, E. Holland, I. M. Pop, N. A. Masluk, T. Brecht, L. Frunzio, M. H. Devoret, L. Glazman, and R. J. Schoelkopf, Reaching 10 ms single photon lifetimes for superconducting aluminum cavities, *Appl. Phys. Lett.* **102**, 192604 (2013).